In-situ synthesis of calcium phosphates derived from eggshells to improve fire improve wood reaction-to-fire properties

Edita Garškaitė

BRANDFORSK
2022:7

BRAND FORSK

Referensgroup

Konrad Wilkens, Flecknoe-Brown Danish Institute of Fire and Security Technology (DBI),
Stefan Särdqvist, Swedish Civil Contingencies Agency (MSB)
Mattias Delin, Brandforsk Foundation.

Brandforsk republishes the project report from LTU, that is published on their website www.ltu.se for reference

"In-situ synthesis of calcium phosphates derived from eggshells to improve wood reaction-to-fire properties"

www.ltu.se

BRANDFORSK
2022:7

In-situ synthesis of calcium phosphates derived from eggshells to improve wood reaction-to-fire properties

Final Report for project No: 2021-013

Brandforsk Funded Application, December 2021
By: Dr Edita Garškaitė (LTU)

Research Team: Dr Edita Garškaitė (project leader), Prof. Michael Försth (LTU) and Prof. Dick Sandberg (LTU)

Cooperation:

Dr **Konrad Wilkens Flecknoe-Brown** (Division of Fire Safety Engineering of Lund University; Danish Institute of Fire and Security Technology (DBI), Denmark),
Prof. **Patrick van Hees** (Division of Fire Safety Engineering of Lund University, Sweden),
Prof. **Jozef Martinka** (Faculty of Materials Science and Technology in Trnava, Slovak University of Technology in Bratislava, Slovakia),
Dr **Peter Rantuch** (Faculty of Materials Science and Technology in Trnava, Slovak University of Technology in Bratislava, Slovakia),
Dr **Marian Drienovsky** (Faculty of Materials Science and Technology in Trnava, Slovak University of Technology in Bratislava, Slovakia),
Dr **Denis Sokol** (Institute of Chemistry of Vilnius University, Lithuania),
Gabija Navašinskaitė (undergraduate student at the Institute of Chemistry of Vilnius University, Lithuania),
Dr **Giedrius Balčiūnas** (Laboratory of Thermal Insulating Materials and Acoustics, Vilnius Gediminas Technical University (Vilnius Tech), Lithuania),
Prof. **Stephen R. Euston** (Institute of Biological Chemistry, Heriot-Watt University, Edinburgh, United Kingdom)

Final Report was written by Dr **Edita Garškaitė** (Wood Science and Engineering, Luleå University of Technology, Skellefteå, Sweden).

Acknowledgement

BrandForsk foundation is greatly acknowledged for the financial support of this project No: 321-013.
We would also like to thank the reference group: Konrad Wilkens Flecknoe-Brown from the Danish Institute of Fire and Security Technology (DBI), Stefan Särdqvist from the Swedish Civil Contingencies Agency (MSB) and Mattias Delin from Brandforsk Foundation. The meetings and discussions with many recommendations have been very valuable.

Content

Abstract

Wood as a natural renewable material is vital for meeting challenges of climate change and ensuring a sustainable future. New technologies, mass-timber systems and environmental benefits bring an increasing interest in high-rise timber buildings world-wide. The regulations require that such wooden structures meet prescribed performance for fire-resistance. The preservative treatment of wood using pressure techniques is an established method, however the challenges such as leachability of the additives and toxicity considerations to human health and environment still remain. The goal of this project is to enhance physicochemical properties of wood by utilising eggshells as a $CaCO_3$ source for bioceramic-reinforced wood materials. Bioceramics are biocompatible materials, *i.e*. not harmful or toxic to living body. Eggshells which consist of about 96% of mineral calcite are, however, considered waste material. The majority of industrially produced eggs are used in the bakery and confectionery, and the eggshells can be easily recycled into e.g. fire retardant production. To an even greater extend, fighting the war against climate change and trying to minimize CO_2 emission, the successful incorporation of mineral calcite within the wood matrix will result in a CO_2 storing hybrid wood material. By combining materials with conflicting properties, we seek to provide solutions to the circular, climate-neutral and sustainable economy.

Background

Interest in employing timber in the construction sector is on the rise and using wood and wood-based materials instead of fossil-based materials to provide the same function can reduce the negative climate impact [1-3]. Thus, the development of wood products by enhancing their physicochemical properties and extending their useful lifetime is an integral part of sustainable production and consumption [4, 5]. The wood-material properties required to be improved are in the first-hand protection against photodegradation, thermal stability or fire retardancy, mechanical properties, resistance to biological degradation, and others [1, 6-8].

A pressing need for safe and efficient fire-retardant materials. The overarching goal of this proposal is to develop viable wood treatment formulations for fire-safe building materials. New technologies, mass-timber systems and environmental benefits bring an increasing interest in timber buildings world-wide. The regulations require that such wooden structures meet prescribed performance for fire-resistance [9]. The flammability of wood and wood-based products can be altered by chemical means using fire and flame retardants. The conventional wood fire-retardant processing techniques involve vacuum-pressure impregnation or applying fire-proof coatings to the wood surface without modifying the intrinsic properties of material [10-12]. The vacuum-pressure impregnation usually proceeds from aqueous solutions that easily diffuse into the wood matrix. Studies showed that many compounds containing boron, phosphorus, aluminum, and nitrogen are to be effective fire retardants [10, 11]. However, despite the fact that the variety of additives were proposed and are used as fire-retardant materials, the challenges such as leachability of the additives and toxicity considerations to human health and environment still remain [10]. The leakage of fire-retardant when the wood products are exposed to elevated moisture conditions could lead to different

behaviour of fire. As a result, the safety of building occupants during a fire event can be restricted. Therefore, the ensuring effective fire performance of wood-products is of vital importance.

Wood is a natural composite material, and the structural components of wood cell wall are mainly cellulose (approximately 40-45%), hemicelluloses (25-30%), and lignin (20-30%) [7, 13, 14]. The chemical composition and hierarchical porous structure of wood offers diverse possibilities for its modification [15]. Lately, studies were conducted to enhance wood properties via "hybrid" modification pathway, namely when impregnation with or without vacuum-pressure is performed from aqueous solutions at ambient temperature and as a chemical reaction proceeds an insoluble solid is coprecipitated within wood matrix when the reactive ions combine [3]. For instance, $CaCO_3$ was successfully synthesised inside the cell-wall structure of beech and spruce wood utilising approach of alkaline hydrolysis of dimethyl carbonate precursors in the presence of calcium ions [16]. In another study, $BaSO_4$ was precipitated within wood scaffold by alternating infiltration with concentrated electrolyte solutions [17]. Preparation of struvite ($MgNH_4PO_4 \cdot 6H_2O$)-wood composite with improved flame retardancy and transverse strength and stiffness under compression was also demonstrated [18, 19]. An incorporation of water-insoluble material within wood matrix, when leaching of intercalated material is prevented, can be a way to make wood firmer and more durable.

Calcium phosphates (CaPs) are a group of minerals widely used in the field of bone tissue engineering [20-22]. They have a similar mineral structure to the main mineral of human bones and teeth. Among them, the most widely investigated are hydroxyapatite ($Ca_{10}(PO_4)_6(OH)_2$, HAP) and tricalcium phosphate ($Ca_3(PO_4)_2$, TCP) [23-25]. Under certain conditions, some of these CaPs are able to transform from one to another, which in consequence determines the density and microstructure of material. Dicalcium phosphate dihydrate, $CaHPO_4 \cdot 2H_2O$ (DCPD), known as brushite (crystallises in the monoclinic space group *Ia* with unit cell parameters a = 5.812(2) Å, b = 15.180(3) Å, c = 6.239(2) Å and β = 116.42(3)°, Z = 4) [26], is formed in dental and urinary calculus[27-29]. It have been shown that brushite mineral (pK_{SP} of 6.59 at 25 °C) is one of the precursors to prepare HAP (pK_{SP} of 116.8 at 25 °C) [30-33]; under treatment with NaOH it immediately transforms into the HAP mineral [34]. It was also reported that DCPD can be transformed into whitlockite ($Ca_9Mg(HPO_4)(PO_4)_6$ or $Ca_3(PO_4)_2 \cdot MgHPO_4$), which has a similar crystal structure to that of β-TCP [35]. Extensive studies were performed to understand CaP formation in solutions (in vitro and in vivo) and variety of techniques were used to assess the nucleation and phase transformation [36-39]. However, to our knowledge, no study on the formation of CaP-based mineral within the wood matrix has been reported. The development of new wood treatment or modification technologies should consider human well-being and should go beyond achieving the lowest possible environmental impact.

CaP bioceramics are conventionally produced by chemical precipitation from aqueous solutions containing calcium and phosphate ions [40-42]. Solution-based chemical synthesis is usually environment-friendly and proceeds at room temperature. Owing to a wide range of precursors, different types of solvents and organic additives (complexing agents, surfactants)

that can be used, such a synthesis offers inexpensive processing way to phase-pure material with desired crystallinity and particle/crystal sizes, which are known to have a profound effect on the material properties, and thereby on the performance of the final product. The synthesis parameters, such as concentration, temperature, pH, reaction time can be also adjusted. Furthermore, CaP minerals exhibit strong ionic and/or covalent bonding which result in their high hardness and compressive strength, high melting points, low thermal and electrical conductivity, and chemical inertness. These unique physicochemical properties make CaPs excellent candidates to be considered as reinforcement material for wood protection. Thus, exploring the synergistic effects of the wood material and CaP minerals, when an insoluble material is formed within wood matrix via wet-chemistry route, might be a worthwhile strategy aiming both low-environmental impact and extend the useful lifetime of the wood-based materials.

Eggshell is a compelling source of calcium [43], as it consist of 96% of mineral calcite ($CaCO_3$), and can serve as a precursor for hydroxyapatite ($Ca_{10}(PO_4)_6(OH)_2$) [44]. According to the EU legislations, eggshell is considered hazardous waste that is disposed of in landfill sites at a high cost. It is predicted that global egg production will increase to about 90 million tons by 2030 [45]. Hence, the established processing methods and the abundance of calcium-rich eggshell-residue makes it a promising lower-cost alternative source for the exploration of new chemical strategies focusing on wood-reinforcement materials.

The main scientific idea of this project was to use the eggshells, a waste from farmed chicken eggs produced for human consumption, as a raw material to reinforce the sapwood of local Scots pine (*Pinus sylvestris* L.) for the improvement of the fire-resistance of wood products. By exploring synergistic effects of low-cost, environmentally friendly and biocompatible materials and desired fire-retardant properties, we propose a sustainable wood-modification principle to increase lifetime and fire-safety of wooden materials

The Project consisted of three parts: **1)** eggshell processing, development of formulations, wood sample preparation, **2)** initial assessment of fire properties and studies of mechanical properties, and **3)** fire testing of cone calorimeter measurements, overall assessment of proposed wood-reinforcement method, and dissemination of results.

Part (1): Eggshell processing, development of formulations, wood sample preparation

1.Experimental

1.1.Materials

Calcium acetate ($Ca(CH_3COO)_2$, 99%, Aldrich) and ammonium dihydrogen phosphate ($NH_4H_2PO_4$, 99%, Aldrich) were used as the cations precursors. Specimens of Scots pine (*Pinus sylvestris* L.) sapwood having sizes of 1 × 1 × 1 cm, 1 × 1 × 15 cm, and 10 × 10 × 1 cm (tangential (T) × radial (R) × longitudinal (L)) were cut from sawn timber obtained from northern Sweden.

1.2.Wood impregnation

To mineralize the wood bocks, 0.5 M, 1.0 M and 1.5 M $Ca(CH_3COOH)_2$ solutions (volume of 1 L) and the corresponding 0.3 M, 0.6 M and 0.9 M of $NH_4H_2PO_4$ solutions (volume of 1 L) were prepared. The reactive solutions were used in the consecutive order that molar ratio of calcium to phosphate ions was maintained to be 1.67. Mineralization of wood blocks was performed in glass round-bottom flasks connected to the vacuum pump. The laboratory setup of the vacuum impregnation is shown in Fig. 1a, b. First, wood specimens were vacuumed for 1 hour to remove the air from the matrix cavities. A 0.5 M $Ca(CH_3COO)_2$ solution was then injected into the flask and the wood blocks were left under vacuum for 2 hours to achieve complete saturation of wood matrix. In a following step, these impregnated specimens were removed from the solution and dried for 3 days at room temperature. Dried specimens were then placed additionally in a round bottom flask connected to the vacuum pump and vacuumed for 1 hours. After the air was removed, a 0.3 M $NH_4H_2PO_4$ solution was injected into the flask. Soaking of wood blocks was performed for 2 hours to allow complete saturation of wood matrix. Magnetic stirrer was used to ensure homogeneous ion distribution within the solution. Turbidity of the solution was observed as well as precipitate formation on the surface of wood blocks. By the end of impregnation procedure, the wood blocks were settled on the bottom of the beaker. Saturated wood blocks were then removed from turbid solution and left for 3 days to dry at room temperature and allow maturation of Ca-P-O precipitate within the wood matrix. In all series of experiments, the same order of solution accession was maintained. The mineralized wood specimens prepared using commercial reagents from the systems of 0.5 M $Ca(CH_3COO)_2$ and 0.3 M $NH_4H_2PO_4$, 1.0 M $Ca(CH_3COO)_2$ and 0.6 M $NH_4H_2PO_4$, and 1.5 M $Ca(CH_3COO)_2$ and 0.9 M $NH_4H_2PO_4$ are designated as DCPD(1)-wood, DCPD(2)-wood and DCPD(3)-wood.

Impregnation of larger wood samples was performed in the desiccator connected to the vacuum pump (Fig. 1c, d).

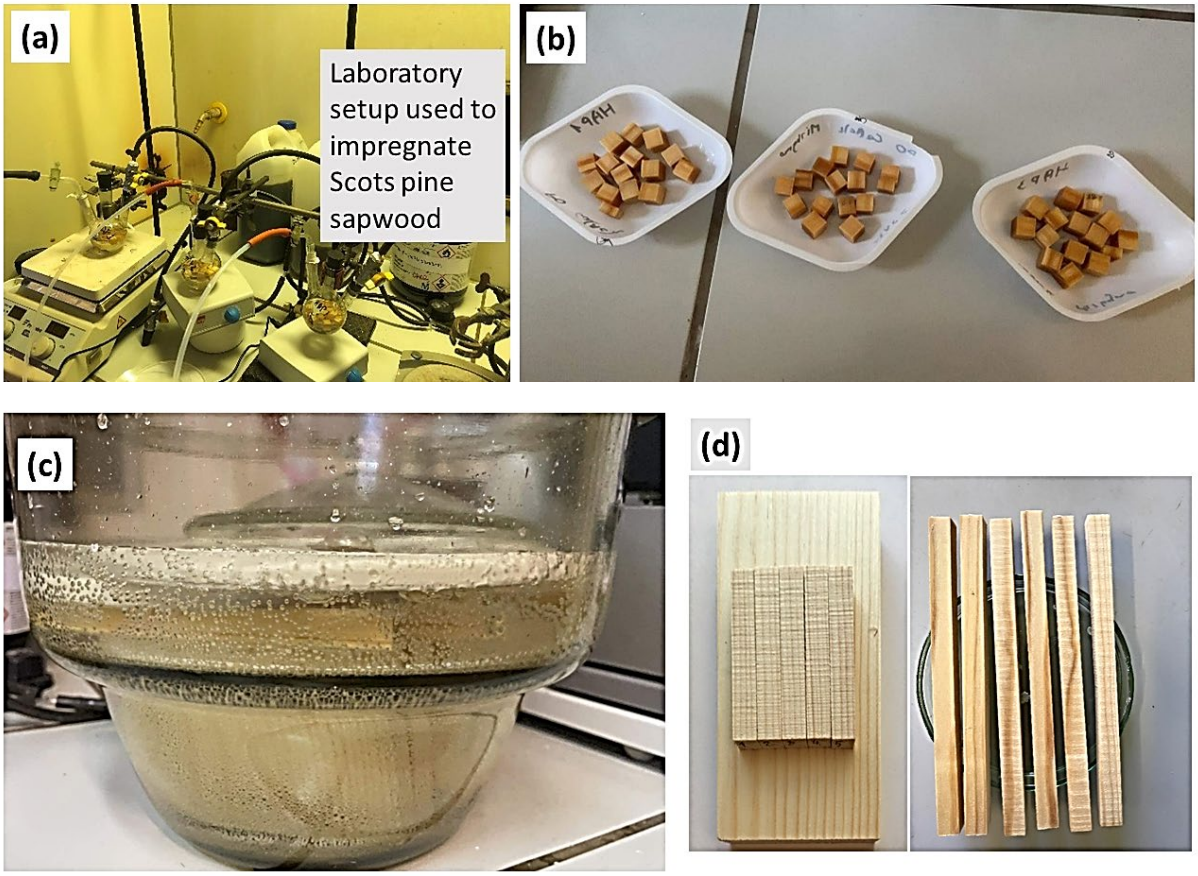

Fig. 1. Camera images of the (a) laboratory setup used to impregnate Scots pine sapwood, (b) sapwood samples impregnated using glass round-bottom flasks shown in (a), (c) sapwood blocks in a desiccator during the impregnation process, and (d) larger wood specimens before the impregnation using desiccator connected to the vacuum pump.

1.3. **Characterization**

Scanning electron microscopy/energy-dispersive X-ray spectroscopy (SEM/EDS): morphological features of pure wood and brushite mineralized wood (microtome-cut slabs of 100 µm thick) were evaluated using a field emission scanning electron microscope (FE-SEM, SU70, Hitachi). A secondary electron imaging was used and the electron beam acceleration voltage was 2.0-5.0 kV. Before analysis, the samples were coated with ~ 10 nm layer of Ag. The samples were also studied using a Hitachi TM3000 Tabletop SEM equipped with the energy dispersive X-ray spectrometer (EDS), and the spectrometer was controlled by the INCA software (Oxford Instruments). A backscattered electron detector was applied and the electron beam acceleration voltage was 15 kV. An X-ray acquisition time of 315 s was used to obtain the EDS spectra (number of independent measurements (n) = 3-5 for each feature of interest) and the elemental mapping images. Wood mineralised from solutions derived from eggshells were studied using FEI Quanta 650 FEG field emission gun scanning electron microscope equipped with Aztec software from Oxford Instruments. To generate the images a back-scatter detector (BSD) was used (electron beam energy of 8-15 kV).

Powder X-ray diffraction (XRD): The crystalline material phase composition was evaluated using a PANalytical X'Pert Powder diffractometer (Cu Kα radiation, step 0.02º, exposure time ~96 s per step) over a 2-theta range of 5-85° at room temperature (Heriot-Watt University, Edinburgh, UK). Untreated and mineralised wood samples were studied using a Rigaku powder X-ray diffractometer (MiniFlex II, Cu-Kα radiation, λ = 0.1542 nm, 40 kV, 100 mA, 2θ = 5-70°).

Fourier transform infrared (FTIR) spectroscopy: Infrared spectra were recorded using a FTIR spectrometer (Frontier FTIR, Perkin Elmer, ZnSe/Diamond ATR crystal, DTGS detector, 4000-600 cm^{-1}, 4 scans).

Thermogravimetry (TG) and differential scanning calorimetry (DSC): Calcination temperature of the eggshell powders was studied under pyrolysis conditions in N_2 (up to 855 °C) atmosphere. TG and DSC analyses were performed using a PerkinElmer STA 6000 Simultaneous Thermal Analyzer. Dried samples of 5–10 mg were heated from 25 to 855 °C at a rate of 10 °C min^{-1} in N_2 atmosphere (20 mL min^{-1}).

1.4. Leaching tests of co-precipitated mineral

Testing of the mineral dissolution and leaching from the wood matrix was conducted in water medium on five replicates. Mineralized wood slabs of 100 µm thick were immersed in polypropylene containers with 5 mL of distilled H_2O and kept for 30 min. The wood slabs were then carefully transferred with tweezers into the other containers containing the same volume of distilled H_2O. For each specimen water was changed three times, and the duration of submersion time was 30 min. After the final leaching step each wood slab was placed on the microscopic glass plate and dried for 48 hours at room temperature.

2. Results and discussion

2.1. Processing of eggshells

The chicken eggs purchased from the local supermarket were washed with water by gently brushing the surface of the eggs. After removing the albumen and the yolk from the crashed eggs, the eggshells were additionally rinsed with distilled water and then dried at room temperature for 24 h. FE-SEM micrographs of the dried eggshell surface, presented in Fig. 2, show the topography of the outer side which consist of the inorganic mineral (Fig. 2a) and the inner side (Fig. 2b) - eggshell membrane consisting of the organic matter.

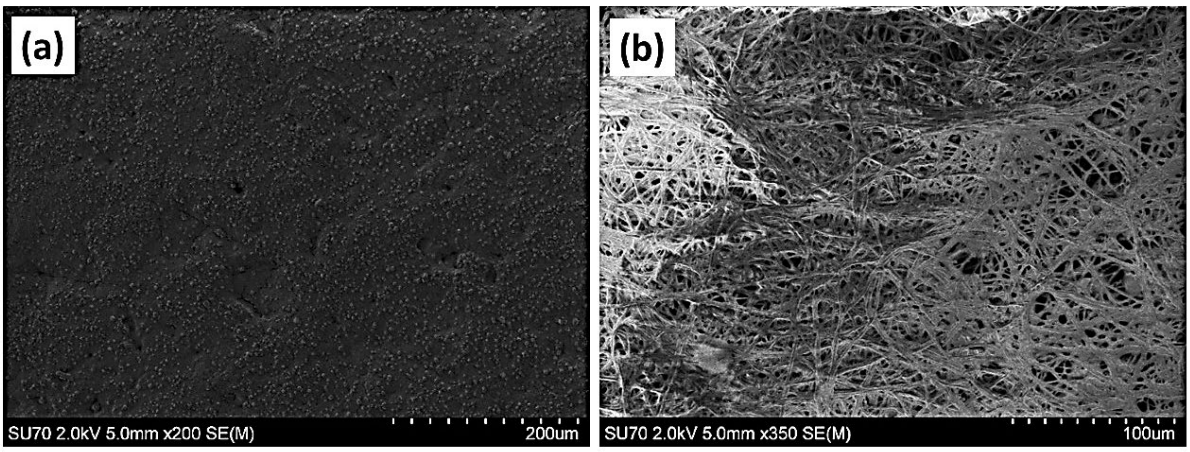

Fig. 2. FE-SEM micrographs of the eggshell surface: (a) outer side consisting of the inorganic mineral, and (b) inner side showing membrane consisting of the organic matter.

The simplified scheme of the eggshell processing is presented in Fig. 3. The dried at room temperature eggshells were grinded in a ceramic mortar and then calcined at 850 °C and 1000 °C for 3 h to obtain calcium oxide (CaO). Calcined CaO powders were additionally grinded in ceramic mortar and then dissolved in an aqueous solution of glacial acetic acid (~50% by volume). Solution was evaporated and dried at 100 °C for 48 h in oven. Obtained white crystals of calcium acetate were further used to impregnate the wood samples.

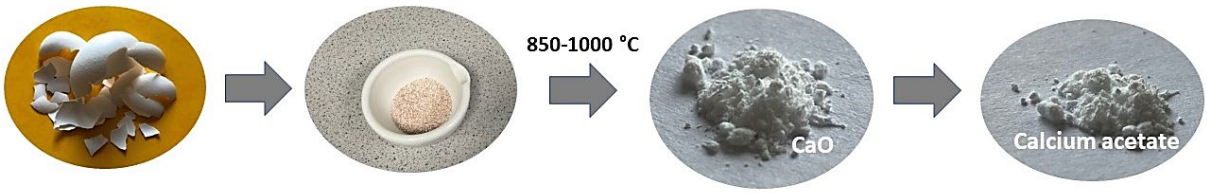

Fig. 3. Simplified scheme of the eggshell processing steps.

TG, DSC and derivative thermogravimetric (DTG) curves for eggshells are presented in Fig. 4. Three main steps of weight loss were clearly seen in the DTG curve. The first very small weight loss of ~0.5% was observed by heating the sample up to 100 °C and assigned to the removal of absorbed water. The second step of weight loss (~2.5%) occurred in the range of 300-350 °C (max. at ~300 °C, DTG curve). This loss can be attributed to the release of volatile components such as CO, CO_2, H_2O, and small molecular compounds containing nitrogen due to decomposition of organic material present within eggshells (membrane). Heating to 850 °C produced an additional ~44% weight loss (max. at 774 °C, DTG curve) and simultaneously exothermic reaction (DSC curve) with a max. at 750 °C. This loss was assigned to CO_2 release due to decomposition of $CaCO_3$ [46, 47]. The decomposition of the eggshells was completed at ~ 800 °C and the inorganic residue mass was 52%.

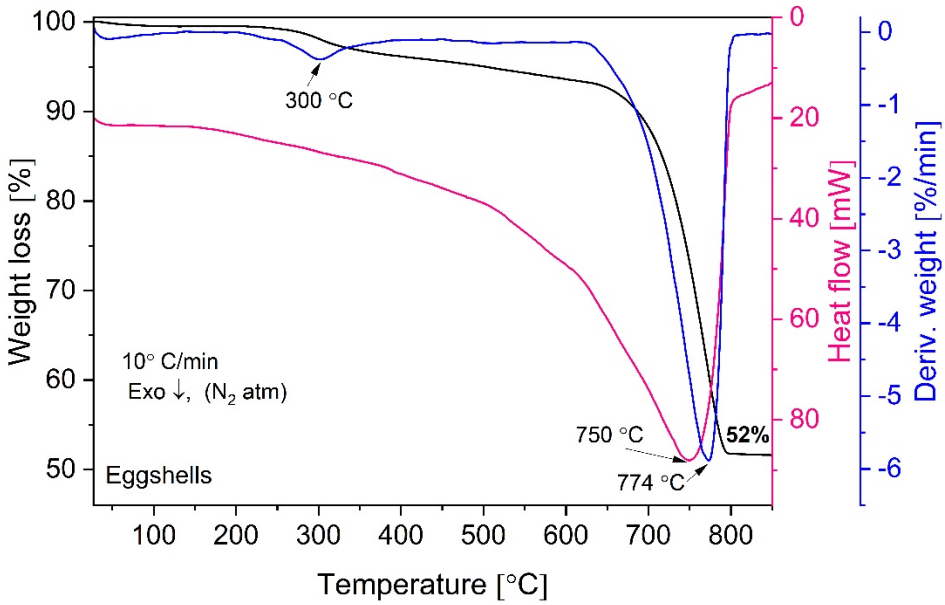

Fig. 4. TG/DSC and DTG curves of the eggshells.

FTIR spectrum of the eggshell material calcined at 850 °C is shown in Fig. 5. The spectrum exhibits characteristic bands to the OH and carbonate (CO_3^{2-}) groups. The strong sharp band with a maximum at 3642 cm^{-1} was assigned to the O–H stretching of the calcium hydroxide ($Ca(OH)_2$) due to absorption of moisture in the sample by CaO [48]. The broad band with maxima at 1465 cm^{-1} and 1416 cm^{-1} could be assigned to the carbonate ions due to vibrational modes of C–O bond. This is consistent with data reported in the literature [44, 49, 50].

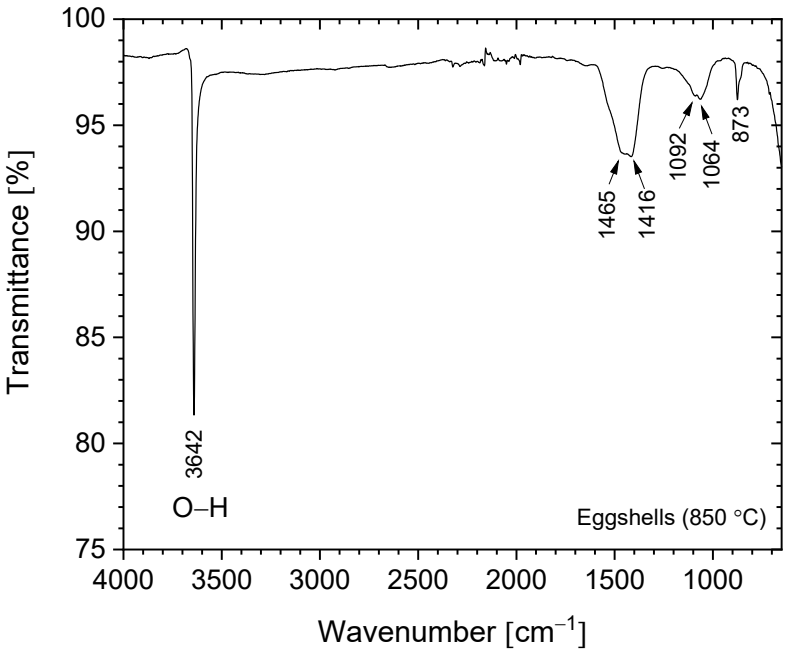

Fig. 5. FTIR spectrum of the eggshells calcined at 850 °C.

XRD analysis confirmed that eggshells calcined at 850 °C consist of two phases, i.e. the reflections in the XRD pattern were assigned to the CaO (JSPD # 96-900-8606) and additional phase of $Ca(OH)_2$ (JSPD # 96-152-9753) (data not presented).

FTIR spectrum of the calcium acetate derived from the eggshells is presented in Fig. 6. The IR spectrum exhibited characteristic bands in the region 2850–3320 cm^{-1} due to O–H stretching vibrations. The bands with a maxima at 1445 cm^{-1} and 1416 cm^{-1} were assigned to the symmetric CH_3 bending vibrations, and bands at ~1526 cm^{-1} and 1610 cm^{-1} were attributed to the C–O antisymmetric stretching vibrations. Bands present at ~1032 cm^{-1} are due to CH_3 in–plane bending vibration. Similar results were reported in the literature [51].

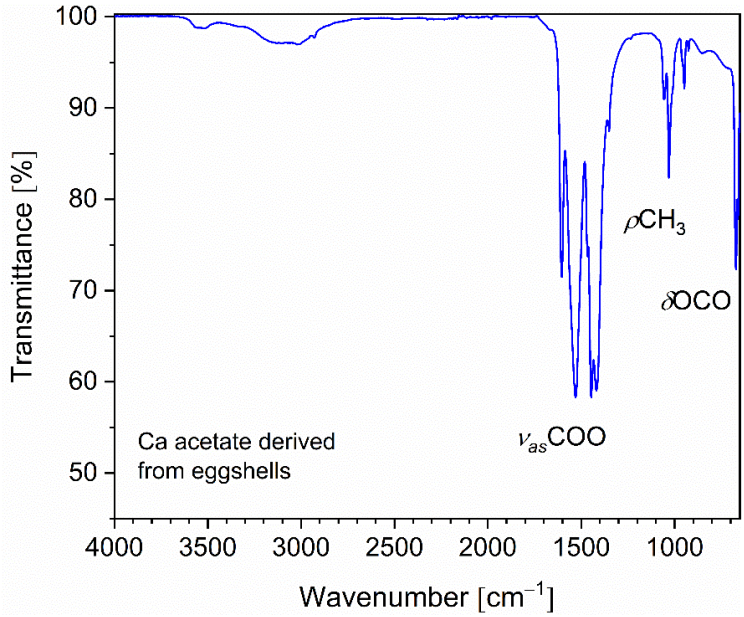

Fig. 6. FTIR spectrum of the eggshell derived calcium acetate.

Samples of Scots pine wood were mineralised from solutions that were prepared using commercial precursors, i.e. calcium acetate and ammonium dihydrogen phosphate, and from solutions of eggshell derived calcium acetate and commercial ammonium dihydrogen phosphate.

2.2. Scots pine wood mineralised from solutions using commercial precursors

The saturation of wood matrix, morphological features and elemental composition of the formed precipitate were assessed by performing SEM/EDS analysis of the cross-sectioned layers of the mineralized-wood blocks. The SEM/EDS images of the representative wood sample mineralized from the $Ca(CH_3COO)_2/NH_4H_2PO_4$ system are presented in Fig. 7. The molar ration of Ca : P was 5 : 3. Examination of the internal cross-sectioned layers showed that the saturation of wood matrix is homogeneous with randomly filled cell lumina (Fig. 7a). The

coprecipitated material exhibited plate-shaped morphology (Fig. 1b), indicating the crystallization of brushite mineral [21, 34, 52]. The cross-section SEM image depicted in Fig. 7c shows EDS-analysed region of the CaP mineralised wood. The elements such as C, P, O, Ca, Al (from the sample holder) and Ag (sputtering prior analysis) were detected (Fig. 7d). The ratios of Ca : P measured of co-precipitated mineral was close to 1. This further indicates a formation of brushite mineral within wood matrix. Various studies have repeatedly shown that phase composition of the CaP mineral strongly depends on the pH of solution where reaction takes place [53-55], and brushite is the most thermodynamically stable phase under acidic conditions (pH between 2 and 6.5) [22, 35, 56]. As the pH of the solution 0.5 M $Ca(CH_3COO)_2$/0.3 M $NH_4H_2PO_4$ system is acidic, the formation of the brushite mineral within wood matrix is expected.

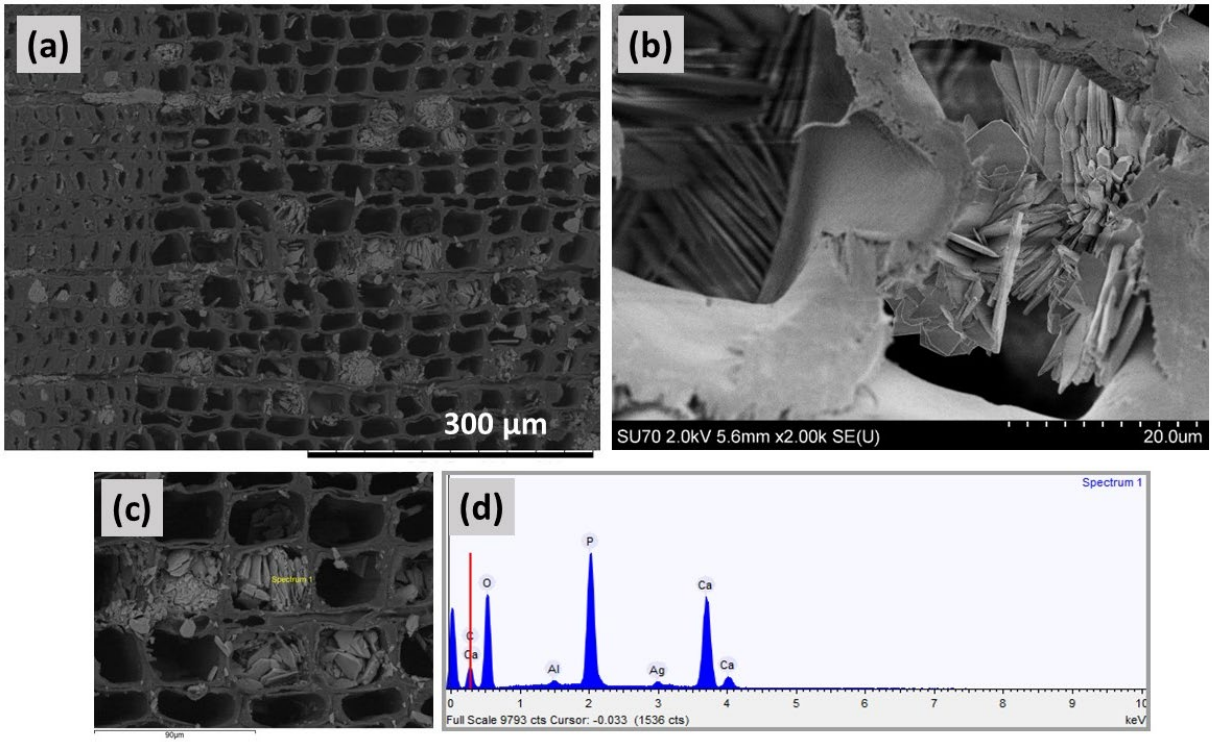

Fig. 7. (a-c) Cross-section SEM images showing morphological features of the mineral co-precipitated within Scots pine wood matrix as well as filling of the lumina, and (d) shows EDS spectrum of the mineral (studied place is shown in (c)).

The minerals crystalized within wood cell lumina from the 1.0 M $Ca(CH_3COO)_2$/0.6 M $NH_4H_2PO_4$, and 1.5 M $Ca(CH_3COO)_2$/0.9 M $NH_4H_2PO_4$ systems exhibited similar morphology, only the saturation of wood matrix slightly increased with an increase in concentration of solutions (data not presented).

Moreover, comparison of layers cut of the modified block surface with those that were cut from the middle of the block, revealed that the saturation of the outermost layers was slightly higher compared to the middle section. This can be ascribed to the higher concentration of reactive species on the wood surface. During the drying of impregnated wood (cycle-I) the migration of $Ca(CH_3COO)_2$ solution through the entire wood block occurs. Subsequently, when wood is treated with the solution containing phosphate ions (cycle-II impregnation) the reaction takes

place instantly, and as more species are available to react, the higher saturation of the cell lumina at the surface of wood block is inevitable.

To evaluate the stability of the precipitated mineral and its intercalation within wood matrix, leaching tests were performed. Fig. 8. shows SEM micrographs with the EDS-based elemental mapping analysis of the wood mineralised from 0.5 M $Ca(CH_3COO)_2$/0.3 M $NH_4H_2PO_4$ system after the leaching. One can observe that co-precipitated mineral remained within wood cell lumina. The plate-like structure of the mineral was also retained. The SEM/EDS mapping analysis also showed that CaP mineral is intercalated within wood cell walls and it remains after the leaching.

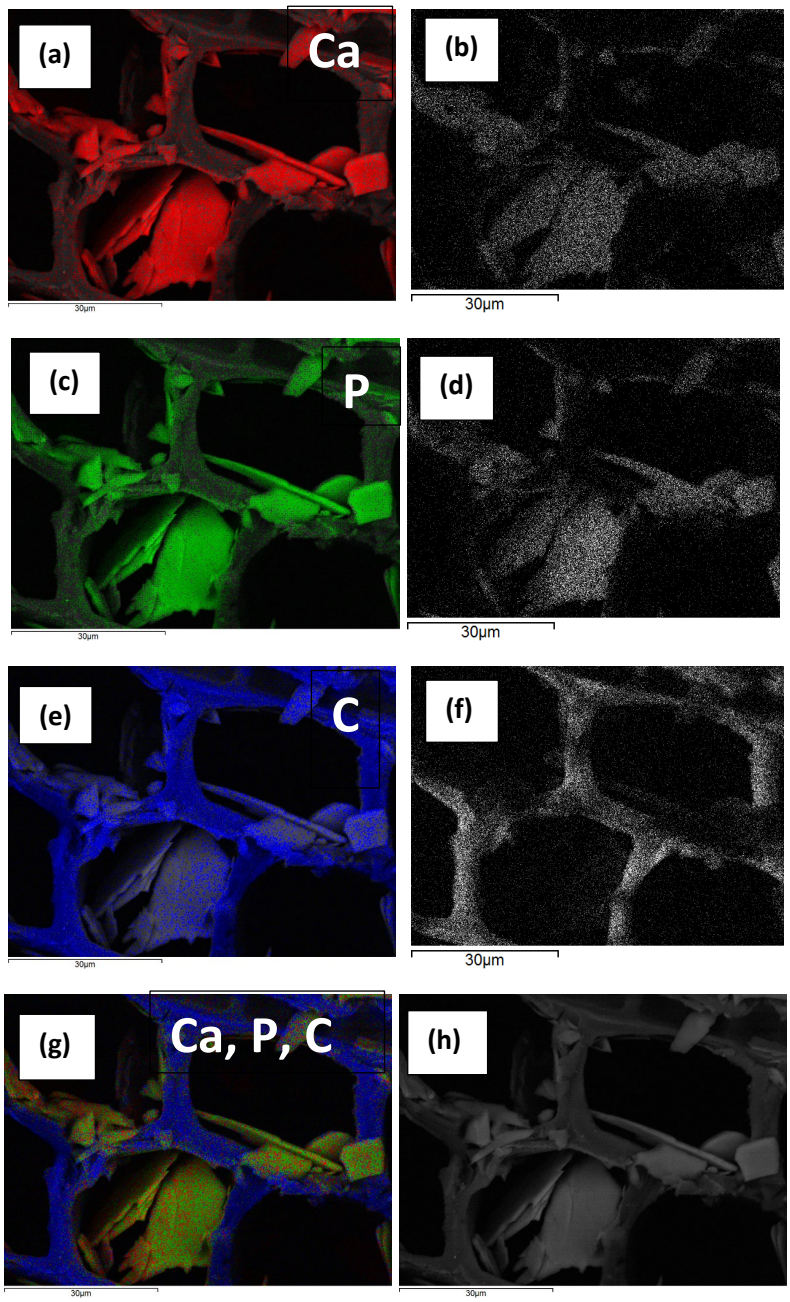

Fig. 8. (a-h) SEM BEI (backscatter electron images) showing (a-g) EDS-based elemental mapping of wood mineralised from 0.5 M $Ca(CH_3COO)_2$/0.3 M $NH_4H_2PO_4$ solution system after the leaching tests

and a distribution of individual elements (designated EDS mapping colours: Ca – red, P – green, O – blue; EDS-based elemental mapping images of Ca, P and C in grayscale are shown in (b), (d),and (f) images, respectively).

Chemical composition of the mineralized wood as well as an integration of CaP mineral within wood matrix was evaluated using FTIR analysis. IR spectra of the untreated wood and brushite-mineralized wood are presented in Fig. 9, and the assignment of the bands for modified wood is summarised in Table 1. The spectrum from the untreated Scots pine wood showed typical absorption bands that are assigned to the main chemical components of wood, i.e. cellulose, hemicellulose and lignin [7, 57]. The bands located in 2940-2840 cm^{-1} region originated from the C–H asymmetric stretching in methyl and methylene groups of aliphatic hydrocarbons [7]. In the 1750-1540 cm^{-1} region, the lignin gives characteristic IR absorption bands. The carbonyl (C=O) stretching vibrations of unconjugated ketones and esters were present at 1740-1710 cm^{-1} (maximum at 1735 cm^{-1}), and conjugated carbonyl structures of lignin absorbed radiation in 1690-1620 cm^{-1}. At lower wavenumbers, such as 1508 cm^{-1} (the aromatic skeletal vibrations of lignin), 1450 cm^{-1} (C=C, C–H, O–H in plane deformation, $–CH_3$ asymmetric bending (lignin)) and 1419 cm^{-1} (C–H aromatic skeletal vibrations (lignin), $–CH_2$ bending deformation (cellulose)) were also present. The fingerprint 1150-950 cm^{-1} region exhibited bands due to various polysaccharide vibrations [7, 57, 58].

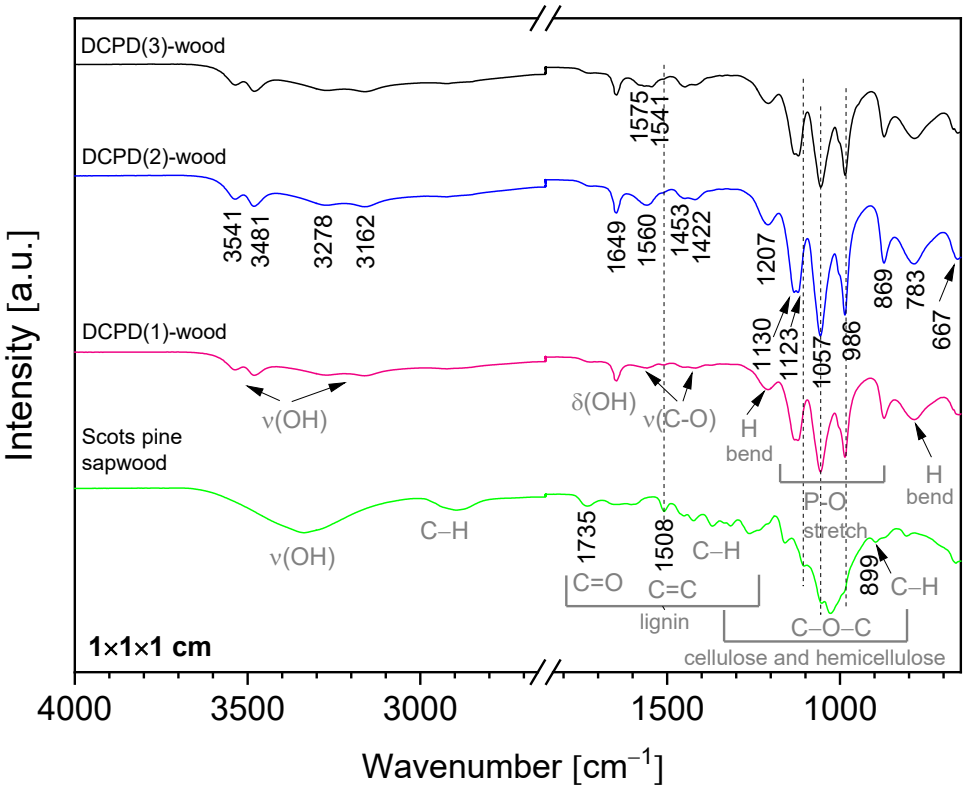

Fig. 9. FTIR spectra of the untreated Scots pine sapwood and the brushite-mineralized wood ('dash' black line indicates position of the band maxima for the untreated wood).

IR spectra of the brushite-mineralized wood exhibited different spectral features. The clearly distinguishable absorption peaks observed at ~1207, 1125 (appearing as doublet at

1130,1123 cm^{-1}), 1057, 986 and 869 cm^{-1} are characteristic of brushite: the vibrations that occur due to the movement of H atom of the HPO_4 group are present at 1207 cm^{-1}, while the P–O stretching vibrations of HPO_4 group gives bands in the 1150-850 cm^{-1} region [29, 59-62]. The broad band present at ~ 783 cm^{-1} could be assigned to overlapped bands attributed to the lignin (C–H out of-plane bending vibrations) and HPO_4 group (P–O–H out of plane bending) [7, 61]. In the spectra of mineralized wood, water vibrations, i.e. internal vibrations and libration modes, were also observed. The broad absorption bands in the region of 3600-3150 cm^{-1} (appearing as doublets at 3541, 3481 cm^{-1} and 3278, 3162 cm^{-1}) are assigned to the O–H stretching modes of the crystal water molecules [29, 31, 61, 63, 64]. The band detected at 1649 cm^{-1} was assigned to the H–O–H bending vibrations, and the broad band at ~ 667 cm^{-1} to the H_2O librational mode [29, 61, 63, 64]. Furthermore, the bands located in the 1610-1520 cm^{-1} and 1480-1380 cm^{-1} regions could be assigned to the C–O stretching modes of carboxyl (COO^-) groups of $Ca(CH_3COO)_2$ molecules [65, 66]. The FTIR spectrum of wood sample treated solely with the 0.5 M $Ca(CH_3COO)_2$ solution (Fig. 10.) shows distinctive bands at 1551 cm^{-1} (1604 cm^{-1} sh) and 1417 cm^{-1} (1449 cm^{-1} sh) that are due to the asymmetric ν(C–O) and symmetric ν(C–O) modes of acetate, respectively [65, 66].

Table 1. IR mode frequencies (in cm^{-1}) and assignment for the brushite-mineralized Scots pine sapwood (the position of bands corresponds for the DCPD(2)-wood sample, Fig. 9).

Frequency (in cm^{-1})	**Vibrating species**	**Reference**
3541, 3481	H_2O, stretch, (crystal water)	[29, 31, 61, 63, 64]
3278, 3162	H_2O, stretch, (crystal water)	[29, 31, 61]
1649	H_2O bending	[29, 31, 61, 63, 64]
1571, 1541	COO^- group, ν, antisymmetric C–O stretching mode (acetate)	[65, 66]
1453, 1422	COO^- group, ν, symmetric C–O stretching mode (acetate)	[65, 66]
1207	H-in-plane bending (HPO_4 group)	[29, 31, 61, 62]
1123	P–O stretch (HPO_4 group group)	[29, 31, 61, 62]

1057	P–O stretch (HPO_4 group group)	[29, 31, 61, 62]
986	P–O stretch (HPO_4 group group)	[29, 31, 61, 62]
869	P–O stretch (HPO_4 group)	[29, 31, 61, 62]
783	H-out-of-plane bend (HPO_4 group), P-OH	[29, 31, 61, 62]
667	H_2O libration	[29, 61, 63, 64]

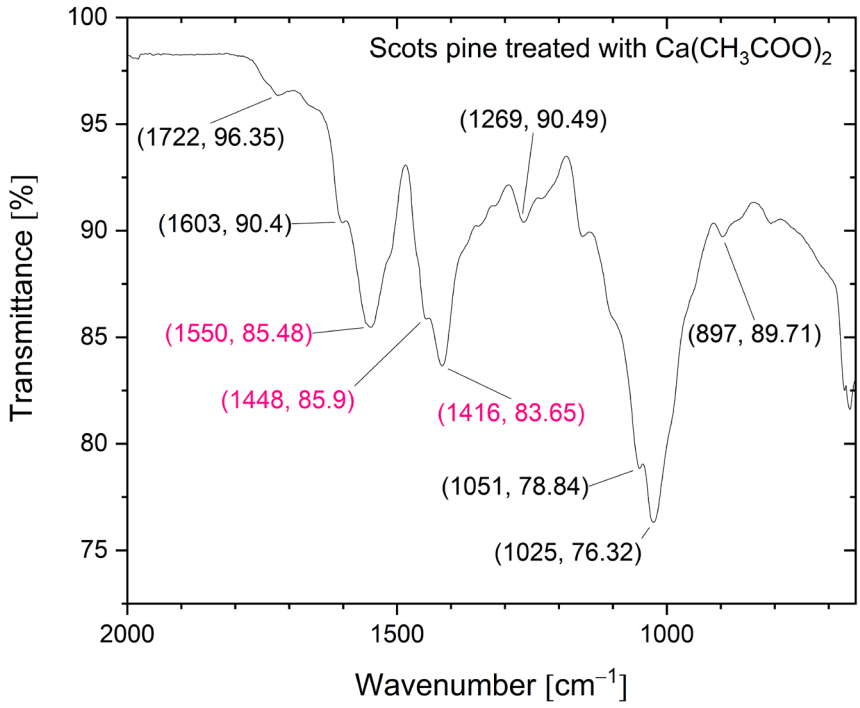

Fig 10. FTIR spectrum of the Scots pine sapwood sample treated from 0.5 M $Ca(CH_3COO)_2$ solution.

2.3. Scots pine wood mineralised from solutions of calcium acetate derived from eggshells and commercial $NH_4H_2PO_4$

The presence of coprecipitated mineral within wood matrix the surface morphological examination of cross-sectioned layers of treated wood blocks was performed. The FE-SEM micrographs of wood mineralised with eggshell derived CaP and the EDS-based elemental

mapping are shown in Fig. 11 and Fig 12, respectively. The SEM micrograph of the internal layer that was cut from the middle of the mineralised wood block (Fig. 11a) of size 1×1×1 cm shows the morphological features of the mineralised wood matrix. The saturation of wood matrix is low and only the random lumina are filled. The surface of wood block (Fig. 11b) exhibits different morphology showing higher amount of the precipitate. One shall also note that the depth gradient was observed when studying layers from the surface and from the middle of the wood block. Layer close to the surface showed more mineralized matrix.

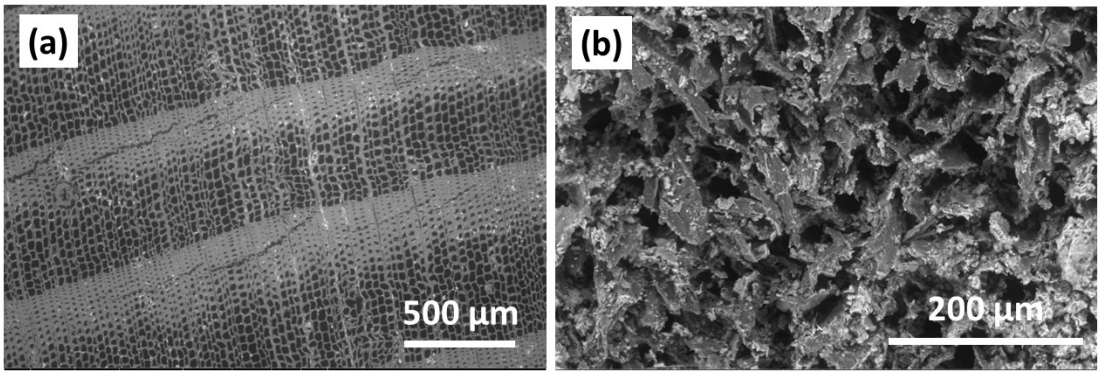

Fig. 11. FE-SEM micrographs of the wood mineralised from solutions of calcium acetate derived from eggshells and commercial $NH_4H_2PO_4$: (a) cross-sectional SEM micrograph of internal layer cut from 1x1x1 cm wood sample, and (b) shows surface of the wood block showing more mineral precipitated within wood matrix.

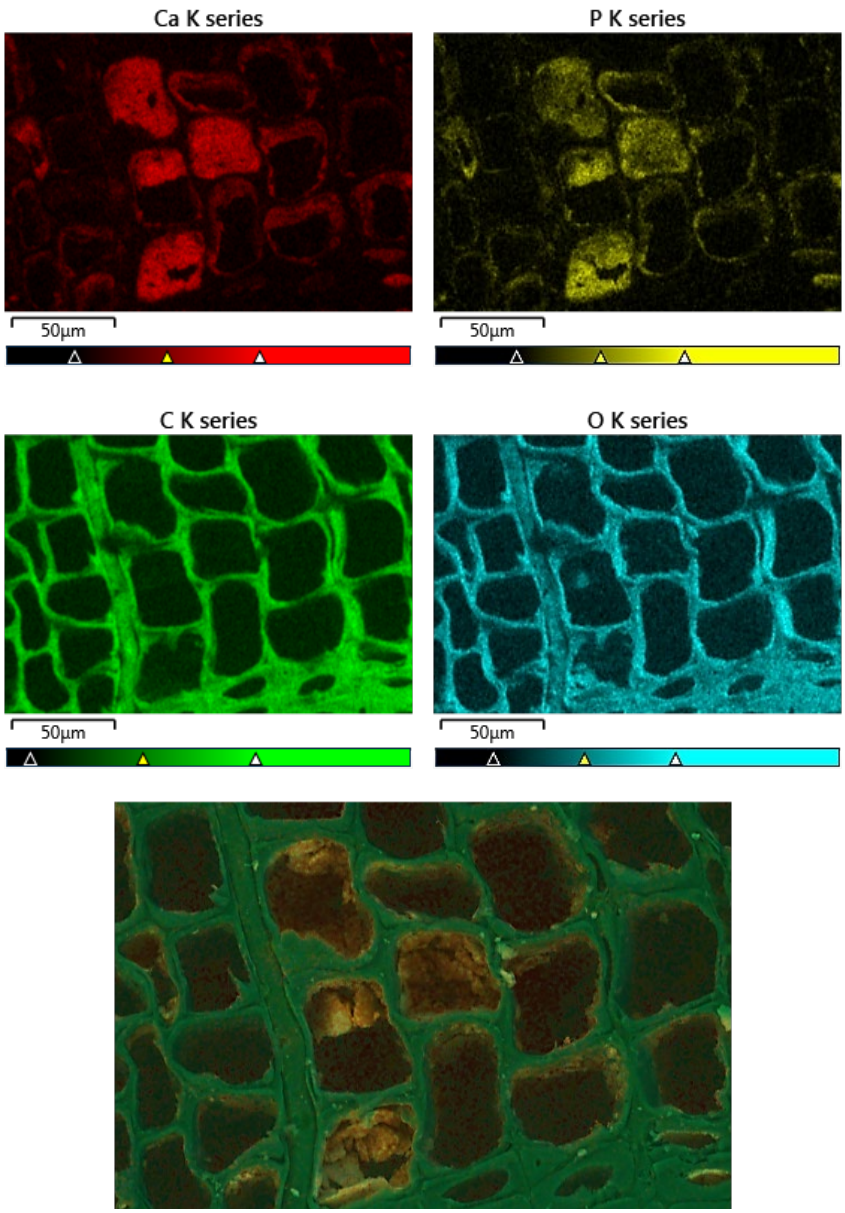

Fig. 12. SEM/EDS mapping images of the HAP-mineralized Scots pine sapwood (microtome cut internal layer of the 1×1×1 cm cube were studied). Eggshell derived from 0.5 M concentration.

The EDS-based elemental mapping was performed to evaluate the wood cell wall saturation with the eggshell derived mineral. The cross-section SEM micrographs depicted in Fig. 12 show EDS-analysed regions of the CaP mineralised wood. The elements such as C, P, O, Ca, Al (from the sample holder) and Ag (sputtering prior analysis) were detected. The individual Ca and P mapping confirmed the saturation of cell wall. The saturation of wood cell wall using aqueous solutions of sodium silicate was demonstrated in our previous studies [7].

Phase composition of formed mineral within wood matrix was examined by powder XRD analysis. XRD patterns of untreated wood and eggshell mineralized wood are shown in Fig. 13. The intensity and width of the peaks in a diffraction pattern indicate the dimensions of the ordered crystallites. XRD pattern of unmodified wood (Fig. 13a) exhibit reflections at $2\theta = 17°$, 22°, 34°, and 45°.The reflections at 17°, 22° and 34° were assigned to the (101), (002) and (040)

diffraction peaks of crystalline cellulose [67]. It is known that cellulose contains both highly ordered (crystalline) and less ordered (semi-crystalline or even amorphous) structures and that wood cellulose tends to be less crystalline than other sources of cellulose. A broad elevation in background ~15–25° was assigned to the amorphous cellulose [7].

Fig. 13b shows XRD pattern of the wood mineralised at room temperature with CaP mineral derived from eggshells. The XRD pattern exhibit different features, the additional small Bragg reflections at $2\theta = 26°$ and region of 32-35° were observed. These reflections in the XRD pattern were assigned to the polycrystalline hydroxyapatite (HAP) which is consistent with literature (JCPDS No. 96-901-4314).

The powders coprecipitated in the desiccator during the impregnation process (cycle-II) were also analysed (Fig. 14). The main strongest reflections in the XRD pattern were assigned to the polycrystalline low crystallinity HAP phase. The reflections arising due to other crystalline phases were also observed. The coprecipitated low crystallinity HAP powders prior the analysis was not washed, and these additional reflections most likely appear due to the initial salts crystallised after the water evaporated from the formed calcium phosphate mineral.

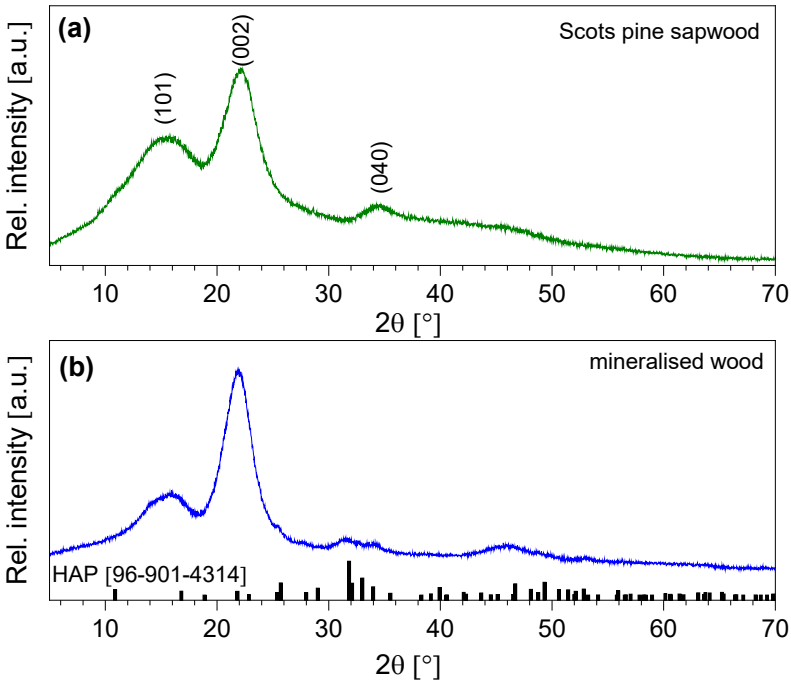

Fig. 13. XRD patterns of the (a) untreated wood and (b) HAP-mineralised wood.

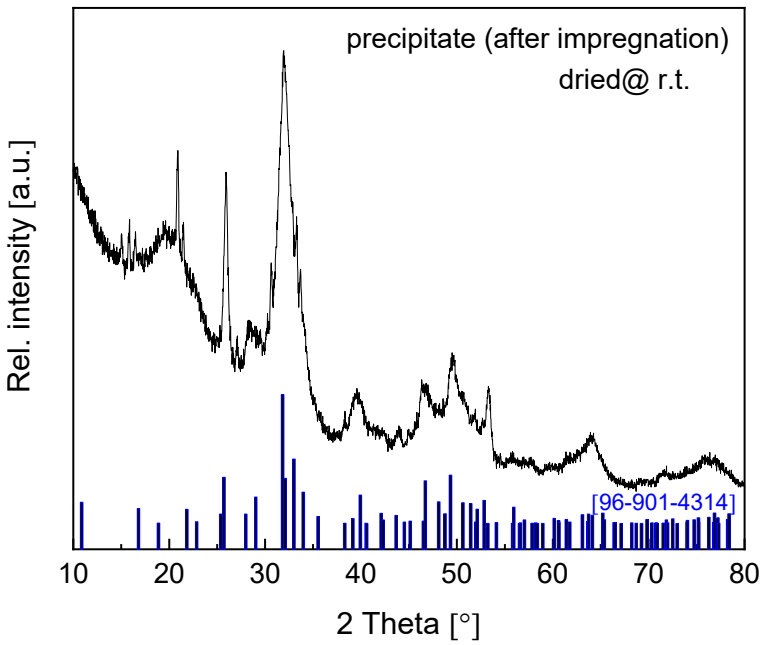

Fig. 14. XRD pattern of powders precipitated during wood mineralization showing reflections assigned to the HAP mineral.

The results herein indicate viability of the wet-chemistry processing route for wood reinforcement with crystalline CaP-based minerals utilising eggshell waste. Results also showed that pH plays important role for calcium phosphate phase.

Part (2): Initial assessment of fire properties and studies of mechanical properties

1. Characterization

Thermogravimetric analysis (TG)/differential scanning calorimetry (DSC) and Thermogravimetric analysis (TG)/differential thermal analysis (DTA)/mass spectrometry (MS): Thermal behaviour of the untreated and mineralized wood was studied under oxidative conditions in air atmosphere (up to 600 °C) and pyrolysis conditions in N_2 (up to 855 °C) and He (up to 1000 °C) atmospheres. Thermogravimetric analysis (TG) and differential scanning calorimetry (DSC) were performed using a PerkinElmer STA 6000 Simultaneous Thermal Analyzer. Dried samples of 5–10 mg were heated from 25 to 855 °C at a rate of 10 °C min^{-1} in N_2 atmosphere (20 mL min^{-1}). Simultaneous Thermal Analyser (Netzsch STA 409CD) equipped with Quadrupole Mass Spectrometer (MS) was used to study samples in synthetic air ($80(O_2)/20(N_2)$) and He atmospheres. For the analysis in air (60 mL min^{-1}) the samples of 3.8 mg were used. The samples were placed in aluminium pans covered with pierced lid in order to enhance contact with synthetic air during the heating (at rate of 10 °C min^{-1}). The measurements performed in He 6.0 atmosphere were with a gas flow rate of 55 mL min^{-1}. The samples (2.5 mg) placed in Al_2O_3 pans were put inside the sample chamber, which was evacuated and purged prior each measurement. The measurements were conducted upon heating between room temperature and 1000 °C with a heating rate of 5°C min^{-1}. A measurement with empty pans (correction) was also made to eliminate background signals from TGA and MS. The MS detector was set to measure atomic mass units from 13 to 313.

Mechanical properties: Impregnated wood specimens of Scots pine (*Pinus sylvestris* L.) sapwood having sizes of 1 × 1 × 1 cm and 1 × 1 × 15 cm (tangential (T) × radial (R) × longitudinal (L)) were used to test compression and bending strength. The compressive strength tests were performed with a universal testing machine Hounsfield H10KS (Hounsfield Test Equipment Ltd, Redhill, UK) and a Qmat Professional software. The cell load was of 10 kN with a resolution of 0.1 N (load measurement accuracy: ± 0.5% of indicated load from 2% to 100% capacity). The load speed was 20 mm/min (position measurement accuracy: 0.001 mm, speed accuracy: ± 0.005% of set speed). To calculate density (ρ), the weight and the linear dimensions of prepared specimens were estimated using precision balance Mettler Toledo MS1003S (e = 0.01 g, d = 0.001 g) and DIGI-MET indicator (e = 0.01 mm, d = 0.001 mm) from Helios Preisser, respectively.

2. Results and discussion

The combustion and pyrolysis of the mineralized wood was also studied. The TG/DSC/DTG curves of the untreated wood and DCPD(1)-wood composite are presented in Fig. 15. The results show that thermal decomposition in oxidizing conditions for the untreated wood progress in three main steps leaving about 6% carbonaceous residue at ~500 °C. The first weight loss of about 5% was observed at temperatures up to 100 °C (maximum at 67 °C, DSC curve) and was attributed to the evaporation of a surface-bound water. An additional weight loss of

55% occurred upon further heating up to 350 °C following strong exothermic peak at ~340 °C. This loss could be attributed to the degradation of hemicelluloses and cellulose, and the removal of volatile components such as CO, CO_2, H_2O and low molecular weight hydrocarbons. Hemicellulose has an amorphous structure, whereas cellulose is semi-crystalline polymer and this leads to its higher thermal stability [68]. Heating to 515 °C produced an additional 34% weight loss and simultaneously exothermic reaction (DSC curve) with a maximum at 470 °C which is mainly related to the decomposition of lignin. Lignin is more thermally stable than hemicellulose and cellulose due to its aromatic structure; the decomposition starts slowly over a wider temperature range (150-900 °C). The decomposition of the untreated wood was completed at ~ 500 °C.

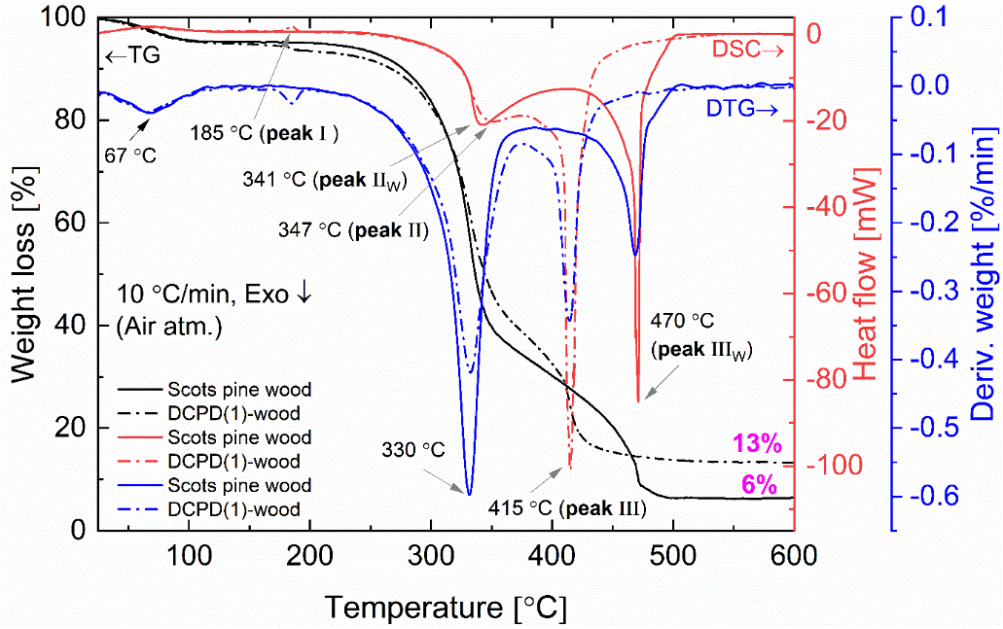

Fig. 15. TG/DSC and DTG curves (oxidative atmosphere) of the untreated and DCPD(1)-mineralized Scots pine sapwood.

Brushite-mineralized wood exhibited different thermal behaviour. The TG/DSC/DTG curves of the DCPD(1)-, DCPD(2)- and DCPD(3)-wood samples showed that thermal degradation of mineralized wood in an oxidative atmosphere proceeds in four steps (Fig. 15 and Fig. 16). One can observe that heating the samples up to 200 °C resulted in two weight-loss events. The first ~5% weight loss (maximum at ~67 °C, DTG curve) was observed up to 100 °C (release of adsorbed water) and the second small weight loss (up to 3%) appears in the temperature range of 170-200 °C with a small endothermic event (maximum at ~186 °C, DSC curves). The latter event was attributed to the removal of water chemically-bonded to wood matrix as well as to initial dehydration of brushite molecules. In fact, literature shows that brushite starts to dehydrate at around 80 °C resulting into a gradual transformation of brushite to monetite ($CaHPO_4$) and formation of an amorphous phase [69, 70]. The third weight loss (~48%, 47% and 38% for the DCPD(1)-, DCPD(2) and DCPD(3)-wood, respectively) takes place up to 375 °C, whilst the last weight loss appears at ~50 °C lower temperature (between 375 °C and 440

°C) compared to the untreated wood. The changes in thermal behaviour were most likely due to the alteration of wood material induced by the acidic medium during the treatment. Furthermore, the residual mass of the material after the burn-off was 7%, 11% and 24% higher for the DCPD(1)-, DCPD(2) and DCPD(3)-wood samples compared to that of the untreated wood indicating that treatment had a significant effect on the mass change. Moreover, after releasing of absorbed water at ~67 °C another dehydration occurred with enthalpy values 15.2 mJ mg^{-1} (peak I, 185 °C) for DCPD(1)-wood, 22.2 mJ mg^{-1} (peak I, 186 °C) for DCPD(2)-wood, and 61.4 mJ mg^{-1} (peak I, 187 °C) for DCPD(3)-wood. The untreated wood exhibited no such dehydration at this temperature (Fig. 15). The huge exothermic reactions on DSC curves (double peak starting at approx. 250 °C) also remain coupled with main mass decrease on TG curves. High amount of heat is released during this burning process, i.e. 5.13 J mg^{-1} (peak II + peak III) for DCPD(1)-wood, 5.26 J mg^{-1} for DCPD(2)-wood, 4.13 J mg^{-1} for DCPD(3)-wood, and 4.96 J mg^{-1} (peak IIw + peak IIIw) for the untreated wood.

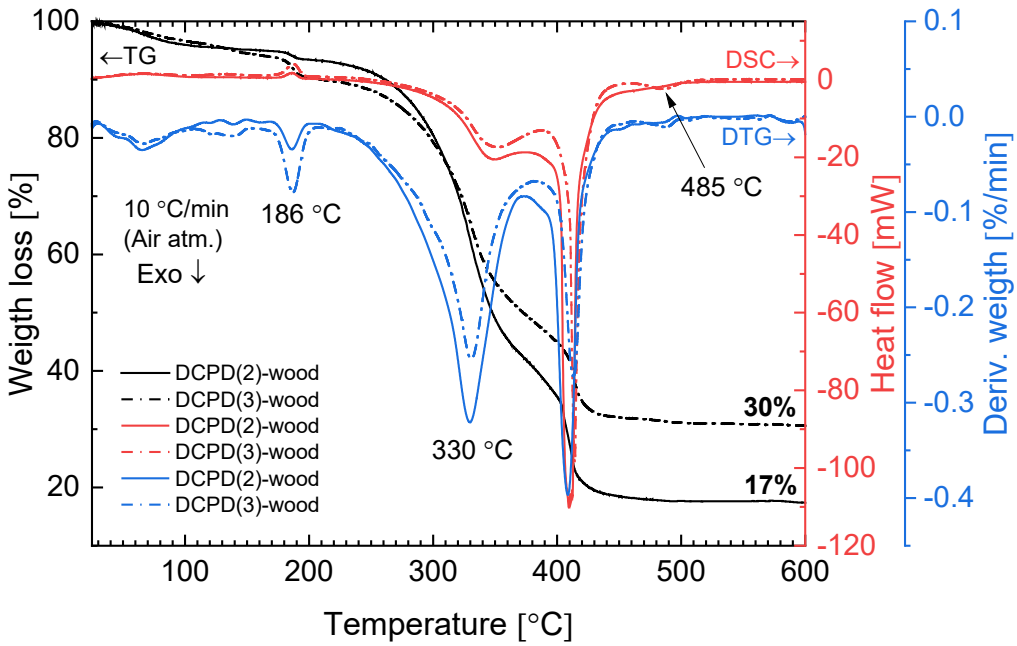

Fig. 16. TG/DSC and DTG curves of DCPD(2)-wood and DCPD(3)-wood composites.

To comprehend the thermal degradation and gain additional information on the material dehydration, mineral phase transition as well as volatile products released during the degradation and final residues the TG/DSC/DTG and TG/DTA coupled with MS analyses were performed for the brushite-mineralized wood samples under pyrolysis conditions. The TG/DTG and DSC curves of the DCPD(1)-wood composite (Fig. 17a) show that thermal decomposition under pyrolysis conditions progresses in four main steps. The first weight loss was observed at temperatures up to 100 °C, and a second weight loss occurred upon further heating the samples up to 200 °C (a small endothermic event with a peak max. at 188 °C). These were attributed to the removal of water and to the dehydration of mineral present within wood matrix. The third weight loss of ~55% for DCPD(1)-wood sample takes place up to 380 °C and can mainly be assigned to the decomposition of large complex carbohydrate molecules, starting with hemicelluloses around 200 °C, and the removal of CO and CO_2 as the major components as

well as H_2, CH_4, C_2H_4 and H_2O as the minor components [7, 71]. The cellulose pyrolysis occurs at higher temperatures (315-400 °C), while lignin, as mentioned previously, decompose slowly over a wider temperature range (150-900 °C) [71, 72]. In addition, the volatile products like NH_3, H_2O and CO_2 can evolve due to the thermal decomposition of initial inorganic salts [73, 74]. Heating to 855 °C led to 18% decrease in weight and this was attributed to the further degradation of organic components of wood and the formation of char (a solid residue left after the devolatilization is complete). The phase transformation within the ceramic also proceeds in this temperature region and such events can be seen with small changes in the DCS curve (around 550 °C and 700 °C). The loss of lattice water associated with formed mineral also appears as $CaHPO_4$ upon pyrolysis at higher temperatures transforms into pyrophosphate ($Ca_2P_2O_7$) and H_2O [75]. The remaining solid residue consisting of the carbon-rich and calcium phosphate-based materials was 17%. A similar thermal behaviour was observed for the brushite-wood composites prepared from solutions of higher concentration. TG/DTG and DSC curves (Fig 17b, c) showed a correlation between initial concentration of the solution and the mineral content, i.e. the remaining solid residue after the burn-off at 855 °C was ~ 21% and 28% for DCPD(2)-wood and DCPD(3)-wood samples, respectively (inset in Fig. 17a). In addition, the thermal behaviour of the surface layer of the mineralized wood blocks was also studied. The TG/DTG and DSC curves exhibited similar features and an average residue mass of the DCPD(1)-, DCPD(2)- and DCPD(3)-wood after the burn-off at 855 °C was 24.13 ± 3.15 (data not presented). This result indicates a complete saturation of the Scots pine sapwood blocks with the initial solutions during the cyclic-treatment process and relevantly homogeneous formation of the solid precipitate within the entire wood matrix.

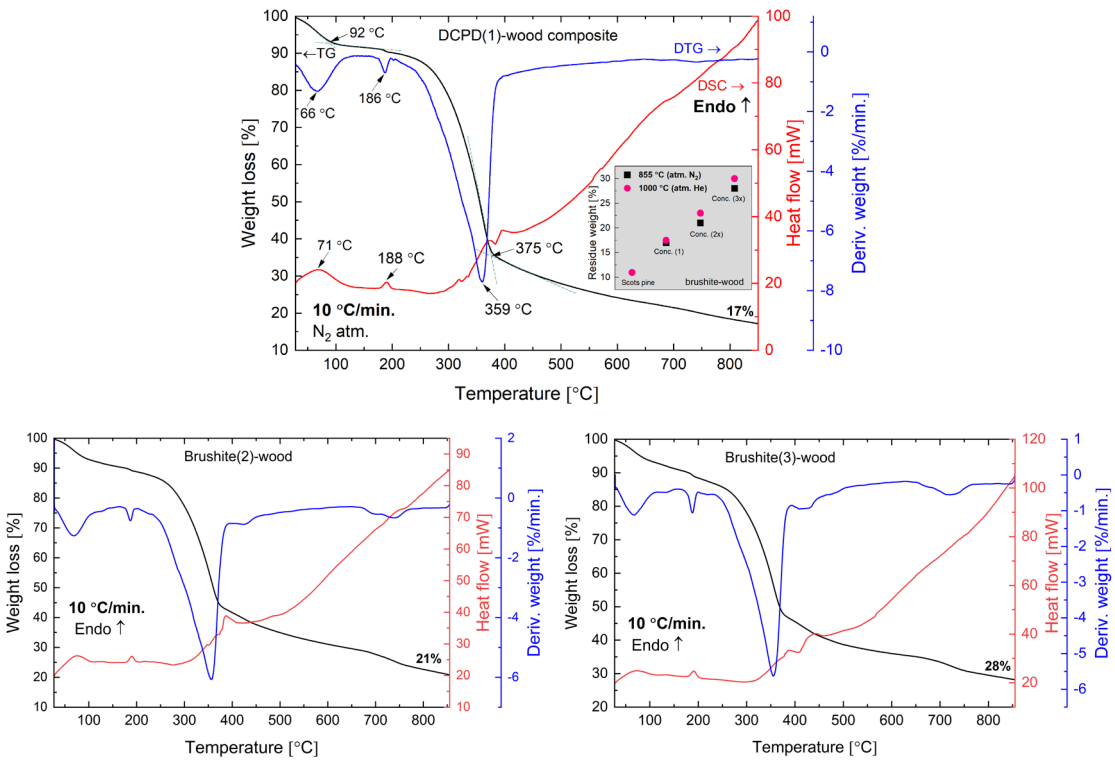

Fig. 17. (a) TG/DTG and DSC curves of (a) the DCDP(1)-wood composite (inset shows residue weight % for the samples after burn when TG analysis was performed in either N_2 atmosphere (10°C/min) or

He atmosphere (5°C/min)), (b) DCDP(2)-mineralized wood, and (c) DCPD(3)-mineralised wood. Specimens taken from the middle of the block of (1×1×1) cm^3 size.

Evolution of volatile products during the thermal decomposition of the brushite-mineralized wood was further evaluated by TG/DTA coupled with MS. Fig. 18. shows the MS curves recorded of the untreated and modified wood, and the corresponding TG/DTA curves are presented in Fig. 19. The MS ion curves for N_2 (*m/z* = 14), H_2O (*m/z* = 17-18), O_2 (*m/z* = 32), C_2O (*m/z* = 39-40), and CO_2 (*m/z* = 44) show peaks that correspond to the individual TGA steps. It can be observed that for the unmodified Scots pine wood sample the major evolution of H_2O, O_2 and CO_2 gases occurs between 250 and 390 °C, and this, as mentioned earlier, can be attributed to the degradation of wood constituents. The MS curves for the brushite-mineralized wood samples exhibited different behaviour. The first significant peak in the MS curves was observed at ~ 190 °C, and it can be assigned to the removal of ammonia and water (NH_3^+/H_2O, *m/z* = 17-18) due to the degradation of ammonia-containing compounds, bound water to the wood matrix as well as to the loss of the crystal water from the brushite molecules. The second peak was observed in the region of 250-380 °C (with maximum at around 350 °C). This could be attributed to the decomposition of the actual wood material. Gas evolution events are consistent with the events observed in the TGA/DTA curves (Fig 19). The third broad peak in the MS curve of NH_3^+/H_2O was detected when heating the materials up to 500 °C and was assigned to the further degradation of the inorganic additives present within the wood matrix. One can also observe that the ratio of peak I (at 190 °C) and peak II (~350-355°C) (Fig. 15) is significantly changing, i.e. the intensity of peak I is increasing with an increase in concentration of inorganic additives. This suggests that initial inorganic chemicals used to treat wood and subsequently formed mineral within wood matrix might be suitable additives aiming to alter thermal degradation behaviour of wood material. The other ionic/molecular species detected in the MS spectra of brushite-mineralized wood exhibited similar evolution patterns. Additionally, the small peaks in the MS curves corresponding to the chemical species of higher molecular weight (*m/z* = 55, and *m/z* = 57) at 355 °C were also observed; these could be due to the organic phase products released during the wood degradation. The residue mass values of the mineralized wood samples studied under different experimental conditions (i.e. heating rate and atmosphere over the sample) were similar (Fig. 17a (inset)). These results indicate that the mineralization of wood when an insoluble material is formed within wood matrix via wet-chemistry route might be a worthwhile strategy seeking both low-environmental impact and enhanced-performance wood materials with tailored properties.

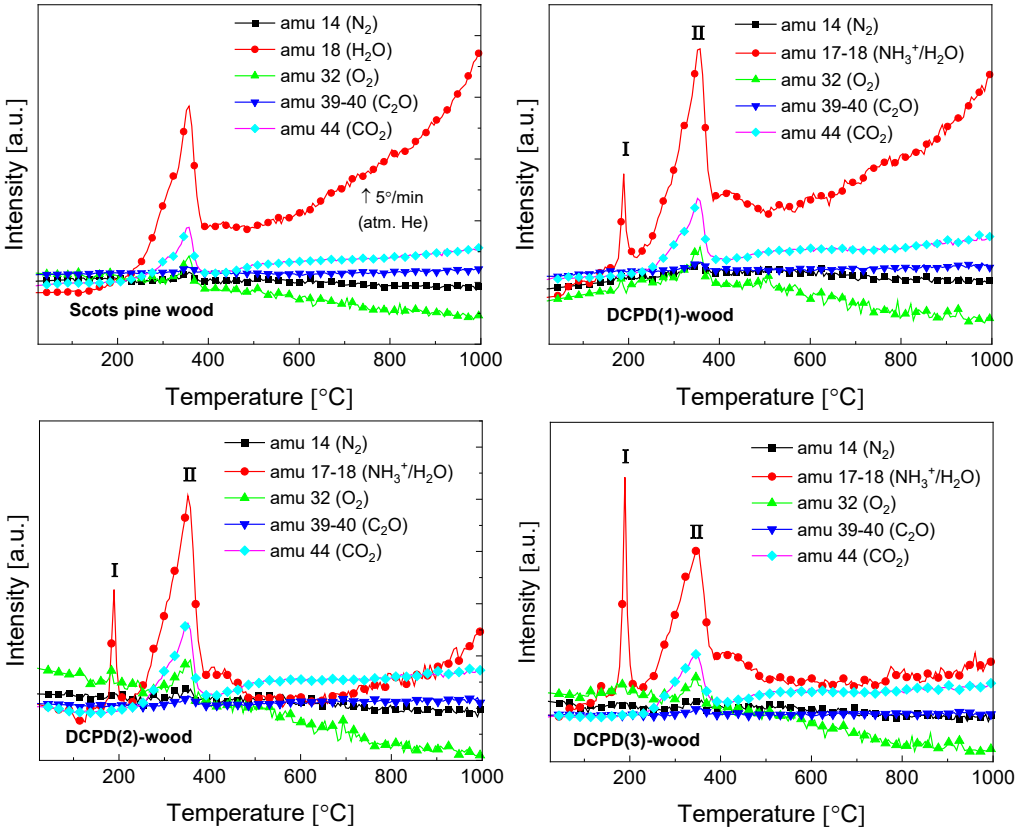

Fig. 18 Brushite wood MS spectra.

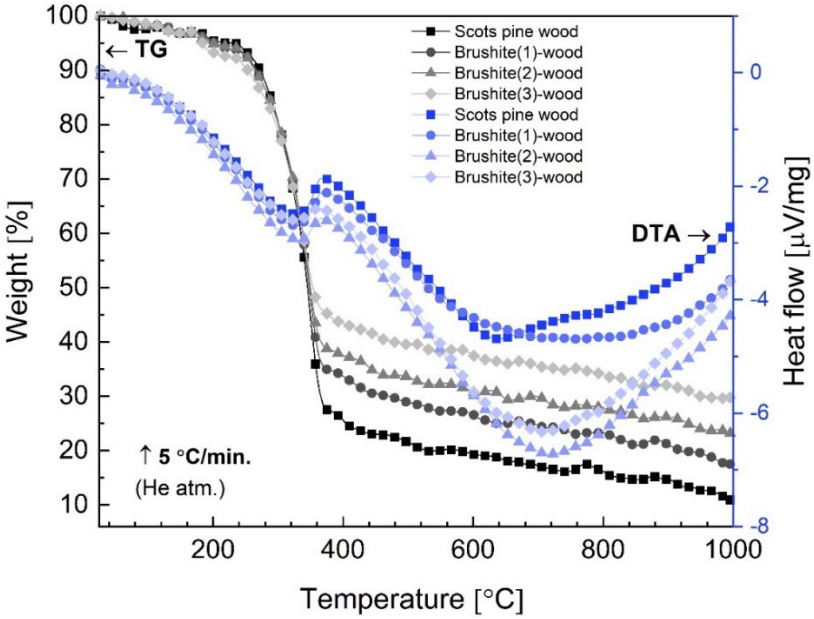

Fig. 19. TG and DTA of the brushite-mineralized Scots pine sapwood (He atm., flow rate 55 mL min^{-1}, Exo=down).

The impact of brushite on the mechanical properties of wood was evaluated by determining compressive and bending strengths. The images of Scots pine wood samples before and after the mineralisation that were used for bending strength tests are presented in Fig. 20. Compressive strength properties of the brushite-mineralized wood were investigated in both

perpendicular and parallel to the fibre directions (Fig. 21a, b). The density of wood increased from 499 to 534, 580 and 634 kg/m^3 for DCPD(1)-wood, DCPD(2)-wood and DCPD(3)-wood specimens, respectively. For compressive strength in the perpendicular to the fibre direction, the strength increased by 20.4%, from 4.9 MPa for untreated wood to 5.9 MPa for DCPD(1)-wood and DCPD(2)-wood specimens. For DCPD(3)-wood specimens the compressive strength was 4.6 MPa. For compression in the parallel to the fibre direction, the strength decreased by 54.0% from 42.1 MPa to 27.3 MPa for DCPD(1)-wood specimens, but slightly increased to 43.7 MPa (by 3.8%) and 44.5 MPa (by 5.7%) for DCPD(2)-wood and DCPD(3)-wood specimens, respectively. The compressive strength test showed that mineralization with brushite did not induce a significant increase or decrease in strength.

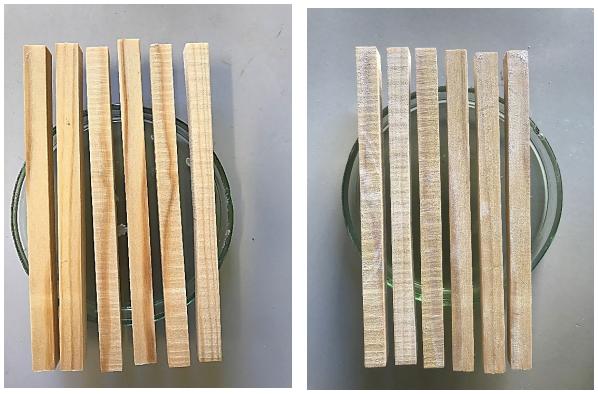

Fig. 20. Wood specimens before the mineralisation and after the impregnation.

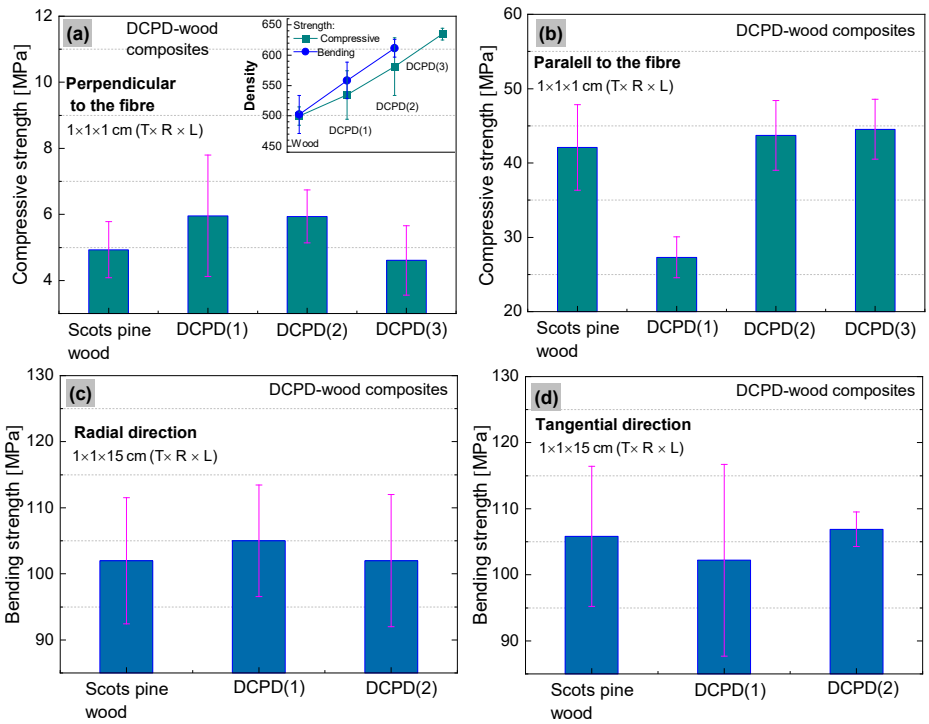

Fig. 21. Mechanical properties: (a, b) compressive strength and (c, d) bending strength of the untreated and the brushite-mineralized Scots pine sapwood samples (Inset: the average density values of the samples).

Regarding the bending strength (Fig. 21c, d), very similar values were obtained for the mineralized wood as compared to the untreated wood. The bending strength in the radial direction was 102 MPa for the untreated wood, and 105 MPa and 102 MPa for DCPD(1)-wood and DCPD(2)-wood specimens, respectively. The bending strength in tangential direction was 105 MPa for the untreated wood and 102 MPa and 107 MPa for the DCPD(1)-wood and DCPD(2)-wood specimens, respectively. Guo *et al.* reported struvite-mineralized wood where process included a vacuum impregnation of the KH_2PO_4 and $MgSO_4$ salt solution into the cavities of Norway Spruce (*Picea abies*) wood specimens followed by ammonium fumigation, which ensured mineral struvite precipitation [19]. The reported studies of mechanical properties showed that mineralization had a minor effect on mechanical properties, i.e. compressive strength correlated with the loading direction, while the three-point bending test revealed a decrease in the strength [19]. Such changes in values of compressive and bending strengths for the brushite-mineralized wood might be attributed to the mechanical properties of the actual ceramic material [75-79]. CaP ceramics are brittle materials, and the compressive strength ranges significantly, depending on their composition, crystallinity, particle and crystal sizes and/or porosity, and these are strongly influenced by the material processing conditions [75, 80-82]. On the other hand, wood is anisotropic material with complex structure. The inherent microstructure of wood, density as well as moisture content are highly significant factors in achieving homogeneous saturation of matrix with coprecipitated ceramic material. Thus, structure-sensitive properties of ceramics as well as synergistic effects of materials with conflicting properties, i.e. ceramics and wood, will impact the mechanical behaviour of ceramic-reinforced wood material.

The impact of eggshell derived mineral on the mechanical properties of wood was evaluated by determining compressive and bending strengths. Compressive strength property of the brushite-mineralized wood was investigated in both perpendicular and parallel to the fiber directions (Fig. 22). The mineralization increased the density of wood samples (n = 11) from 499 to 529 kg/m^3, but there was no significant effect on the compressive strength observed. For compression in the perpendicular to the fiber direction, the strength decreased from 4.9 MPa for unmodified wood to 4.2 MPa for CaP-mineralized wood, and strength in compression parallel to the fibre direction decreased from 42 MPa for unmodified wood to 38 MPa for mineralized wood. With respect for the bending strength, the strength in the tangential direction decreased from 102 MPa for unmodified wood to 93 MPa for modified wood, and the strength in the radial direction decreased from 106 MPa for unmodified wood to 85 MPa for modified wood. The density of these samples increased from 502±29 kg/m^3 for the unmodified wood to 555±56 kg/m^3 for mineralized wood. The overall small decrease in strength, both compression and bending, might be associated with the degradation of wood constituents under strong basic medium. An increased pH during the wood modification processing as ammonia was used to adjust the pH of initial solution (pH = 11) that is needed to induce the formation of apatitic phase of mineral. Thus, the studies further shall be undertaken when fine balance between the mineral processing and wood material properties to avoid destruction of the constituents of wood material.

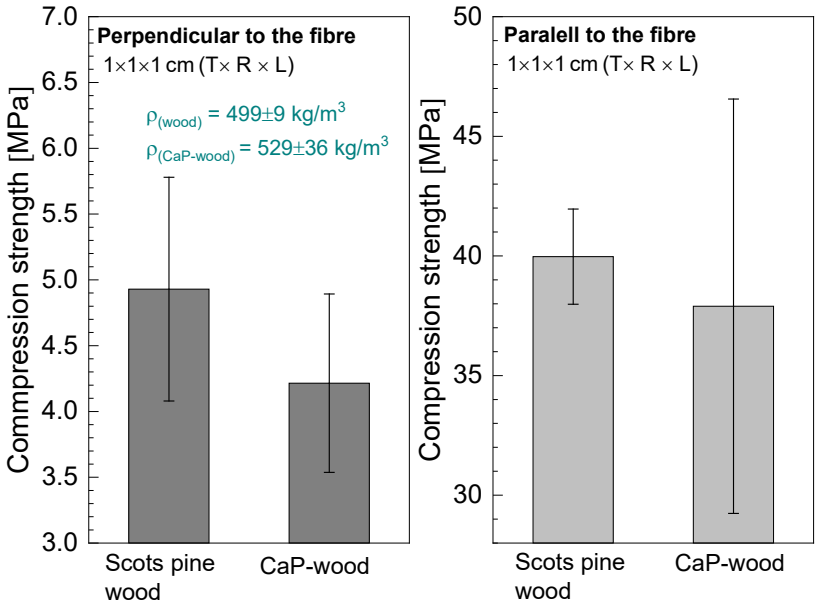

Fig. 22. Mechanical compression strength properties of the untreated and CaP-mineralized Scots pine sapwood.

Overall results imply that proposed wet-chemistry processing route to CaP-based-wood composites opens possibilities for the upscaling, due to its simplicity, low-cost and established industrial wood treatment techniques that are available. This further suggests that if extremely benign and technologically feasible methods, when stable inorganic materials are crystalized within wood cell-wall cavities can be developed, the pristine structure and durability of final-wood product can be retained with relatively good confidence. This is especially attractive for the construction sector.

Part (3): Fire testing – CC and MCC measurements

1. Characterization

Cone calorimeter (CC) testing: Specimens before the analysis were conditioned in a climate chamber (20 °C, 65% relative humidity (RH)) for 5 days. Fire performance of samples was investigated at the Slovak University of Technology in Bratislava, Slovakia, by the cone calorimeter (CC) (Fire testing Technology, Ltd., East Grinstead; the United Kingdom) at two heat fluxes (20 and 50 kW m^{-2}). The cone calorimeter and testing procedure were in compliance with ISO 5660-1:2015 [83]. The cone calorimeter measure mass loss of sample, amount of oxygen consumed, and time to ignition (TTI). These data were used to calculated total heat release (THR) and effective heat of combustion (EHC) in compliance with ISO 5660-1:2015 [83]. From measured and calculated values were calculated other key fire characteristics of investigated samples by following methods (critical heat flux and ignition temperature in compliance with Spearpoint *et al*. [84], maximum average rate of heat emission in compliance with Marquis *et al*. [85], and flashover category in compliance with Kokkala *et al.* [86]).

Microscale combustion calorimeter (MCC) testing: MCC testing was performed at Lund University, Sweden, using the apparatus developed by the US Federal Aviation Administration (FAA). Its primary use is as a flammability assessment-screening tool for new materials [87, 88]. The eggshell-derived HAP-mineralised wood was studied in oxidative and pyrolysis conditions, i.e. synthetic air (80(O_2)/20(N_2) and N_2 atm. with a heating rate of 1°C/s.

2. Results and discussion

The MCC and CC instruments and apparatus principle are presented in Fig. 23. The MCC (Fig. 23b) is based on the principles of pyrolysis and combustion analysis via oxygen consumption calorimetry, employing pyrolysis-combustion flow calorimetry (PCFC) [88]. The sample sizes required in the MCC are in order of milligrams (herein, specimens of ~5 mg were used). During CC testing the specimens of dimensions 10 × 10 cm and of varying thickness are placed under the cone heater and irradiated with the heat source until ignition. CC testing allows to get information on the combustion behaviour of a material, e.g. how fast a sample ignites and burn, and how much heat is released in the process. The time to ignition is measured. Once ignited, the heating is turned off and the time to flameout, i.e. the time it takes for the sample to either self-extinguish or burn completely is measured (Fig. 23c).

Herein, the CC and MCC tests were performed only for the eggshell-HAP-mineralised wood samples. The camera photos of the untreated wood and eggshell-HAP-mineralised wood specimens, depicted in Fig. 24(a-c), show the CaP mineral precipitated on the wood surface. The samples of 10 × 10 × 1 cm (Fig. 24b) were used for CC testing, whilst the samples of 1 × 1 × 1 cm (Fig. 24c) were cross-sectioned with microtome to obtain 100 µm thickness stubs that were further selected and used for MCC measurements.

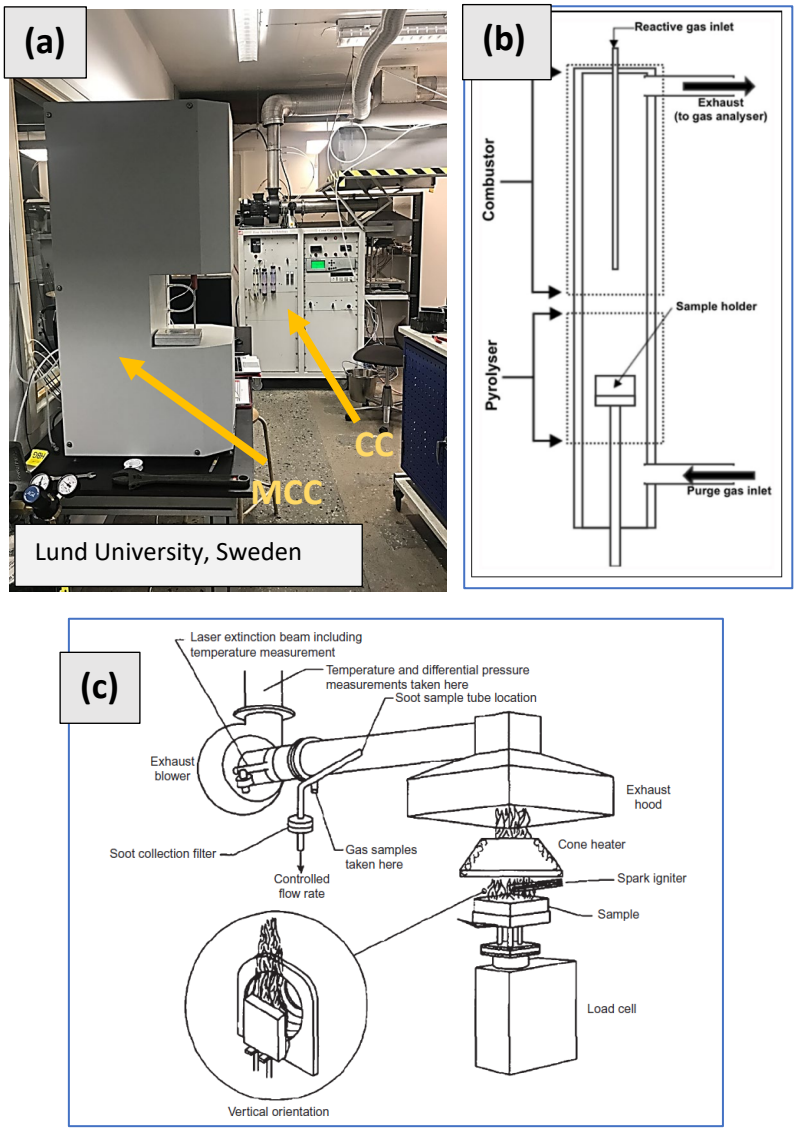

Fig. 23. (a) Camera image showing CC and MCC instruments, and simplified schematic of (b) MCC and (c) CC instruments principle [87, 88].

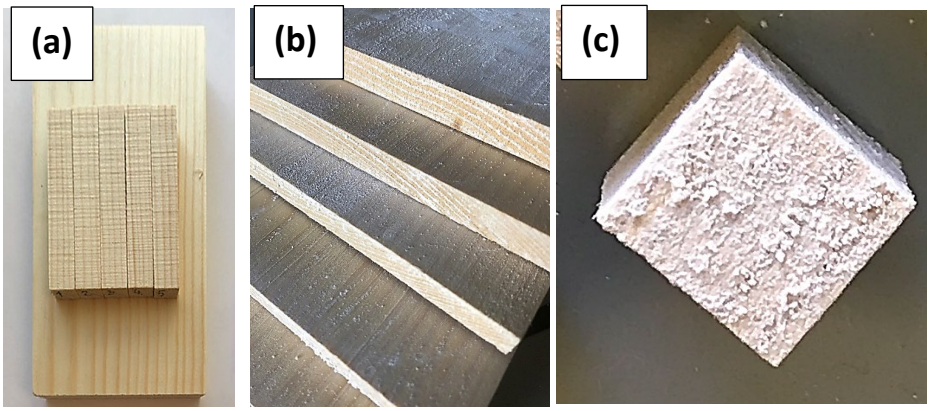

Fig. 24. Photos of wood samples (a) before the treatment and (b, c) after the cyclic impregnation exhibiting morphological changes - co-precipitated HAP mineral derived from eggshells on the surface of wood blocks.

Studying the 100 µm stubs gave us a possibility to estimate the mineral content within the entire wood block. The MCC tests performed in N_2 atm. show a decrease (~20%) in the peak HRR/g value for the surface sample tested (Fig. 25). MCC data (in N_2 atm., n = 3 for the same specimen studied) also show that there is a difference between the sample from the surface and internal layer of the wood block, suggesting the mineral concentration gradient within the entire wood block and so that the impregnation of the sample is not consistent throughout the sample across section.

Looking at the HRR curves (MCC in air atm., n = 1 for the same specimen studied), shown in Fig. 25b, one can observe the similarity of the Scots pine wood results to those obtained from the TGA tests: DTG vs MCC results look quite similar, and the peak values are approximately the same (Fig. 15). Although it is also interesting to note that the second peak is earlier in the MCC (HRR maximum at 417 °C) compared to the TGA (maximum at 470 °C, DSC curve (Fig. 15). Regarding the eggshell-HAP-mineralised wood, different MCC results were obtained. One can observe that HRR curve has a very different shape and seems to join the two reactions seen in the Scots wood sample together. This might be due to the induced changes in the actual wood material due the treatment and removal of extractives from the wood matrix due to base solution (pH was = 10-11). On the other hand, the co-precipitated CaP and residue salts might act as a catalyst of the second reaction (second peak in HRR curve) and so result in continuous heat release. Furthermore, the residue char left after the burn-off was negligible for unmodified wood, whilst ash content for the egg-HAP-wood was 4.9%, indicating that mineral-wood composite possesses the higher density compared to the untreated wood, and this agrees with TGA data described in the previous paragraphs. We shall note that this is initial results and additional studies required to fully evaluate fire-retardancy properties of the mineralised wood.

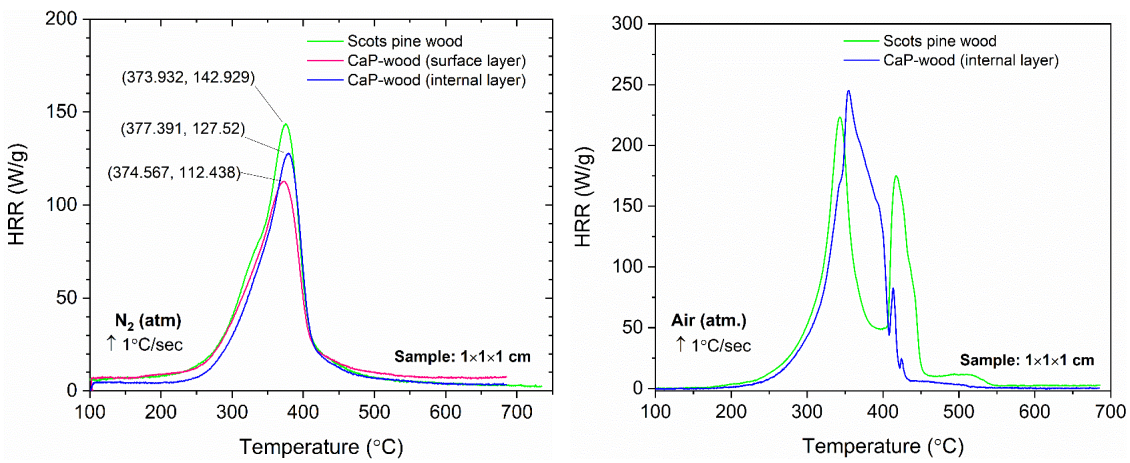

Fig. 25. MCC HRR curves of the eggshell-HAP-mineralised wood: (a) tests were performed in N_2 atmosphere and (b) in a synthetic air atm.

The CC test further provided an insight into the fire behaviour developing by presenting various important parameters, including heat release rate (HRR), total heat release (THR), mass loss, time to ignition (TTI), etc. The CC data obtained for the untreated Scots pine wood and eggshell-HAP-mineralised wood are presented in Table 2.

Table 2. CC data for the untreated Scots pine wood and the eggshell-HAP-wood specimens.

Properties	Heat flux (kW m^{-2})	Reference: untreated wood	Sample: Eggshell-HAP-wood
Time to ignition (s)	20	120±7	250±35
	50	23±3	28±3
Critical heat flux (kW m^{-2}) calculated in compliance with Spearpoint [84]	NA	17±2	22±1
Ignition temperature (°C) calculated in compliance with Spearpoint [84]	NA	388±25	442±10
Time to flashover (s) calculated in compliance with Kokkala [86]	NA	120 to 600	120 to 600
Maximum heat release rate (kW m^{-2})	20	197±3	199±33
	50	273±13	252±26
Maximum average rate of heat emission (kW m^{-2})	20	97±4	80±6
	50	157±2	152±2
Total heat release (MJ m^{-2})	20	94±11	91±2
	50	115±4	105±12
Effective heat of combustion (MJ kg^{-1})	20	16.22±0.77	15.29±0.70
	50	17.85±0.28	16.92±0.05
Maximum mass loss rate (kg m^{-2} s^{-1})	20	16.45±1.70	19.28±0.09
	50	20.13±0.21	21.36±0.57
Average mass loss rate (kg m^{-2} s^{-1})	20	3.30±0.25	3.31±0.13
	50	3.76±0.07	3.57±0.33

HRR is considered the most important parameter to evaluate the growth and spread of the fire. CC HRR and THR curves (Fig. 26) showed that the major impact of the mineral for the wood material was a delay in ignition time which can be seen in the tests performed under external heat flux of 20 kW/m^2. The HRR curve shape is rather similar, and this indicates that the mineral work as a heat sink. The similar behavior was observed for aluminum trihydroxide (ATH, $Al(OH)_3$) [89]. Moreover, the mineralized wood samples exhibit similar behaviour during CC tests and MCC tests, i.e. the second peak under heat flux of 50 kW/m^2 starting sooner compared to the untreated wood. To confirm the course of this event the further studies shall be undertaken. Furthermore, the THR is reduced for both heat fluxes slightly (Fig. 26b, d). Overall, one can observe that the treated wood behaves rather similar as untreated. The second peak in the HRR curves is related to the cracks in the wood.

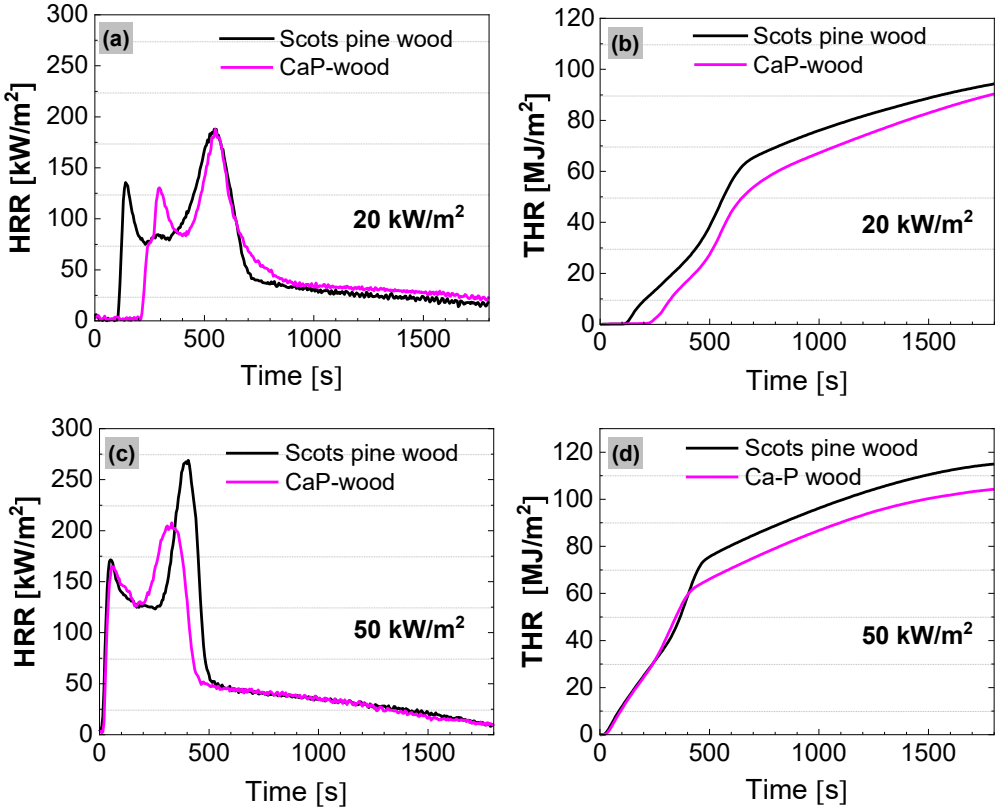

Fig. 26. Cone calorimeter data: HRR and THR curves of the eggshell-HAP-wood composites (tests were performed under external heat flux of 20kW/m^2 and 50 kW/m^2).

CC and MCC results showed that mineral intercalation into wood matrix show positive effects on wood protection against thermal degradation. This further suggests that if extremely benign and technologically feasible methods, when stable inorganic materials are crystalized within wood cell-wall cavities can be developed, the pristine structure and durability of final-wood product can be retained with relatively good confidence. This is especially attractive for the construction sector.

Conclusions

- The results indicate viability of the wet-chemistry processing route for wood reinforcement with crystalline calcium phosphate(CaP)-based minerals utilising eggshell waste.
- CaP mineral, precipitated within wood matrix by wet-chemistry route proposed herein, does not induce a significant change in mechanical strength (compression and bending) properties.
- Thermogravimetric analysis and mass spectroscopy: the identification of evolved gaseous species showed relatively enhanced water release from the mineralized wood thereby implying the material fire retardancy properties.

- CC and MCC showed reduced HRR and THR which indicates potential of minerals as reinforcement material for protection of wood products against fire.
- Results imply that proposed wet-chemistry processing route to CaP-based-wood composites opens possibilities for the upscaling, due to its simplicity, low-cost and established industrial wood treatment techniques that are available.
- Overall results imply a potential in producing hybrid bio-based materials that could be attractive in the construction sector as an environmentally friendly building material.

Suggestions for further work

1) Optimization of eggshell material processing (emphasis on synthesis and processing parameters such as temperature, pressure, impregnation time, material phase, crystallinity and phase purity, etc.).
2) Wood-mineral composites (optimization of the impregnation pathway, homogeneous mineralisation of the entire wood block).
3) Upscaling.
4) Fire engineering/properties (upscaling, evaluation of smoke release via light extinction method using diode lasers)).
5) Economic assessment.

Scientific publications in progress

Submitted: E. Garskaite, et al. (2022) *RSC Advances* journal. Manuscript includes data about the brushite mineralised Scots pine (*Pinus Sylvestris* L.) sapwood.

In preparation and to be submitted to an international journal *Edita Garskaite et al.* The scientific manuscript will include data about the calcium phosphate mineral derived from chicken-eggshell waste, wood mineralisation and fire properties of hybrid CaP-based composites that were evaluated by performing CC and MCC measurements.

Conference(s)

This project was presented at the EFB 2022 (European Federation of Biotechnology) Virtual conference, 4-5 October, 2022, Poster: Edita Garskaite "*Studying the application of agricultural and aquaculture wastes as wood protection materials*" (ID 1126) (Abstract book, p. 37).

References:

1. Ramage, M.H., et al., *The wood from the trees: The use of timber in construction.* Renewable and Sustainable Energy Reviews, 2017. **68**: p. 333-359.
2. Howard, C., et al., *Wood product carbon substitution benefits: a critical review of assumptions.* Carbon Balance and Management, 2021. **16**(1): p. 9.
3. Berglund, L.A. and I. Burgert, *Bioinspired Wood Nanotechnology for Functional Materials.* Advanced Materials, 2018. **30**(19): p. 1704285.
4. Bonfield, P., *Environmental Performance Enters Construction Materials.* MRS Bulletin, 2008. **33**(4): p. 454-456.
5. Dakwale, V.A., R.V. Ralegaonkar, and S. Mandavgane, *Improving environmental performance of building through increased energy efficiency: A review.* Sustainable Cities and Society, 2011. **1**(4): p. 211-218.
6. Burgert, I., et al., *Bio-inspired functional wood-based materials – hybrids and replicates.* International Materials Reviews, 2015. **60**(8): p. 431-450.

7. Garskaite, E., et al., *Surface hardness and flammability of Na2SiO3 and nano-TiO2 reinforced wood composites.* RSC Advances, 2019. **9**(48): p. 27973-27986.
8. Popescu, C.-M. and A. Pfriem, *Treatments and modification to improve the reaction to fire of wood and wood based products—An overview.* Fire and Materials, 2020. **44**(1): p. 100-111.
9. Östman, B., *National fire regulations for the use of wood in buildings – worldwide review 2020.* Wood Material Science & Engineering, 2021: p. 1-4.
10. Popescu, C.-M. and A. Pfriem, *Treatments and modification to improve the reaction to fire of wood and wood based products—An overview.* Fire and Materials, 2019. **n/a**(n/a).
11. Lowden, L.A. and T.R. Hull, *Flammability behaviour of wood and a review of the methods for its reduction.* Fire Science Reviews, 2013. **2**(1): p. 4.
12. Lazar, S.T., T.J. Kolibaba, and J.C. Grunlan, *Flame-retardant surface treatments.* Nature Reviews Materials, 2020. **5**(4): p. 259-275.
13. Sjöström E., *Chapter 1 - THE STRUCTURE OF WOOD*, in *Wood Chemistry (Second Edition)*, E. Sjöström Editor. 1993, Academic Press: San Diego. p. 1-20.
14. Toumpanaki, E., D.U. Shah, and S.J. Eichhorn, *Beyond What Meets the Eye: Imaging and Imagining Wood Mechanical–Structural Properties.* Advanced Materials, 2020. **n/a**(n/a): p. 2001613.
15. Ashby, M.F. and D.R.H. Jones, *Chapter 29 - Wood Structure and Properties*, in *Engineering Materials 2 (Fourth Edition)*, M.F. Ashby and D.R.H. Jones, Editors. 2013, Butterworth-Heinemann: Boston. p. 493-508.
16. Merk, V., et al., *Hybrid wood materials with improved fire retardance by bio-inspired mineralisation on the nano- and submicron level.* Green Chemistry, 2015. **17**(3): p. 1423-1428.
17. Merk, V., et al., *Oriented Crystallization of Barium Sulfate Confined in Hierarchical Cellular Structures.* Crystal Growth & Design, 2017. **17**(2): p. 677-684.
18. Guo, H., et al., *Bioinspired Struvite Mineralization for Fire-Resistant Wood.* ACS Applied Materials & Interfaces, 2019. **11**(5): p. 5427-5434.
19. Guo, H., et al., *Struvite Mineralized Wood as Sustainable Building Material: Mechanical and Combustion Behavior.* ACS Sustainable Chemistry & Engineering, 2020. **8**(28): p. 10402-10412.
20. Eliaz, N. and N. Metoki, *Calcium Phosphate Bioceramics: A Review of Their History, Structure, Properties, Coating Technologies and Biomedical Applications.* Materials (Basel), 2017. **10**(4).
21. Boanini, E., et al., *Synthesis and Hydrolysis of Brushite (DCPD): The Role of Ionic Substitution.* Crystal Growth & Design, 2021. **21**(3): p. 1689-1697.
22. Ishikawa, K., *1.17 Bioactive Ceramics: Cements ☆*, in *Comprehensive Biomaterials II*, P. Ducheyne, Editor. 2017, Elsevier: Oxford. p. 368-391.
23. LeGeros, R.Z., et al., *Biphasic calcium phosphate bioceramics: preparation, properties and applications.* J Mater Sci Mater Med, 2003. **14**(3): p. 201-9.
24. Lobo, S.E. and T.L. Arinzeh, *Biphasic Calcium Phosphate Ceramics for Bone Regeneration and Tissue Engineering Applications.* Materials, 2010. **3**(2): p. 815-826.
25. Sinusaite, L., et al., *Controllable synthesis of tricalcium phosphate (TCP) polymorphs by wet precipitation: Effect of washing procedure.* Ceramics International, 2019. **45**(9): p. 12423-12428.
26. Mathew, M. and S. Takagi, *Structures of Biological Minerals in Dental Research.* Journal of research of the National Institute of Standards and Technology, 2001. **106**(6): p. 1035-1044.
27. Prien, E.L. and E.L. Prien, Jr., *Composition and structure of urinary stone.* Am J Med, 1968. **45**(5): p. 654-72.
28. Miller, M.A., et al., *Maturation of Brushite (CaHPO4·2H2O) and In Situ Crystallization of Brushite Micro-Granules.* Advances in Bioceramics and Porous Ceramics VI, 2013: p. 77-91.
29. Hirsch, A., et al., *Infrared Absorption Spectrum of Brushite from First Principles.* Chemistry of Materials, 2014. **26**(9): p. 2934-2942.

30. Tamimi, F., Z. Sheikh, and J. Barralet, *Dicalcium phosphate cements: Brushite and monetite.* Acta Biomaterialia, 2012. **8**(2): p. 474-487.
31. Cama, G., et al., *A novel method of forming micro- and macroporous monetite cements.* Journal of Materials Chemistry B, 2013. **1**(7): p. 958-969.
32. Johnsson, M.S.A. and G.H. Nancollas, *The Role of Brushite and Octacalcium Phosphate in Apatite Formation.* Critical Reviews in Oral Biology & Medicine, 1992. **3**(1): p. 61-82.
33. Mandel, S. and A.C. Tas, *Brushite (CaHPO(4)·2H(2)O) to octacalcium phosphate (Ca(8)(HPO(4))(2)(PO(4))(4)·5H(2)O) transformation in DMEM solutions at 36.5°C.* Mater Sci Eng C Mater Biol Appl, 2010. **30**(2): p. 245-254.
34. Miller, M.A., et al., *Testing of Brushite (CaHPO4·2H2O) in Synthetic Biomineralization Solutions and In Situ Crystallization of Brushite Micro-Granules.* Journal of the American Ceramic Society, 2012. **95**(7): p. 2178-2188.
35. Tas, A.C., *Transformation of Brushite (CaHPO4·2H2O) to Whitlockite (Ca9Mg(HPO4)(PO4)6) or Other CaPs in Physiologically Relevant Solutions.* Journal of the American Ceramic Society, 2016. **99**(4): p. 1200-1206.
36. Termine, J.D., R.A. Peckauskas, and A.S. Posner, *Calcium phosphate formation in vitro: II. Effects of environment on amorphous-crystalline transformation.* Archives of Biochemistry and Biophysics, 1970. **140**(2): p. 318-325.
37. Borkiewicz, O., J. Rakovan, and C.L. Cahill, *Time-resolved in situ studies of apatite formation in aqueous solutions.* American Mineralogist, 2010. **95**(8-9): p. 1224-1236.
38. Okada, M., et al., *Intermediate Water on Calcium Phosphate Minerals: Its Origin and Role in Crystal Growth.* ACS Applied Bio Materials, 2019. **2**(3): p. 981-986.
39. Hoeher, A.J., et al., *Impacts of Initial Ca/P on Amorphous Calcium Phosphate.* Crystal Growth & Design, 2021. **21**(7): p. 3736-3745.
40. Bohner, M., B.L.G. Santoni, and N. Döbelin, *β-tricalcium phosphate for bone substitution: Synthesis and properties.* Acta Biomaterialia, 2020. **113**: p. 23-41.
41. Grigoraviciute-Puroniene, I., et al., *A novel synthetic approach to low-crystallinity calcium deficient hydroxyapatite.* Ceramics International, 2019. **45**(12): p. 15620-15623.
42. Grigoraviciute-Puroniene, I., et al., *A novel synthetic approach for the calcium hydroxyapatite from the food products.* Journal of Sol-Gel Science and Technology, 2019. **91**(1): p. 63-71.
43. Oliveira, D.A., P. Benelli, and E.R. Amante, *A literature review on adding value to solid residues: egg shells.* Journal of Cleaner Production, 2013. **46**: p. 42-47.
44. Ronan, K. and M.B. Kannan, *Novel Sustainable Route for Synthesis of Hydroxyapatite Biomaterial from Biowastes.* ACS Sustainable Chemistry & Engineering, 2017. **5**(3): p. 2237-2245.
45. Mignardi, S., et al., *Valorization of Eggshell Biowaste for Sustainable Environmental Remediation.* Scientific Reports, 2020. **10**(1): p. 2436.
46. Salaudeen, S.A., et al., *Eggshell as a Carbon Dioxide Sorbent: Kinetics of the Calcination and Carbonation Reactions.* Energy & Fuels, 2019. **33**(5): p. 4474-4486.
47. Cree, D. and A. Rutter, *Sustainable Bio-Inspired Limestone Eggshell Powder for Potential Industrialized Applications.* ACS Sustainable Chemistry & Engineering, 2015. **3**(5): p. 941-949.
48. Luna Vera, F., et al., *From Eggshells to Quicklime: Using Carbonate Cycle as an Integrating Concept To Introduce Students to Materials Analysis by TGA and FTIR.* Journal of Chemical Education, 2018. **95**(4): p. 625-630.
49. Sacia, E.R., et al., *Synthesis and Regeneration of Sustainable CaO Sorbents from Chicken Eggshells for Enhanced Carbon Dioxide Capture.* ACS Sustainable Chemistry & Engineering, 2013. **1**(8): p. 903-909.
50. Dadhich, P., et al., *A Simple Approach for an Eggshell-Based 3D-Printed Osteoinductive Multiphasic Calcium Phosphate Scaffold.* ACS Applied Materials & Interfaces, 2016. **8**(19): p. 11910-11924.

51. Garduño-Pineda, L., et al., *Removal of inorganic chemical species and organic matter from slaughterhouse wastewater via calcium acetate synthesized from eggshell.* Journal of Environmental Science and Health, Part A, 2019. **54**(4): p. 295-305.
52. Toshima, T., et al., *Morphology control of brushite prepared by aqueous solution synthesis.* Journal of Asian Ceramic Societies, 2014. **2**(1): p. 52-56.
53. Mekmene, O., et al., *Effects of pH and Ca/P molar ratio on the quantity and crystalline structure of calcium phosphates obtained from aqueous solutions.* Dairy Science & Technology, 2009. **89**(3): p. 301-316.
54. Johnsson, M.S. and G.H. Nancollas, *The role of brushite and octacalcium phosphate in apatite formation.* Crit Rev Oral Biol Med, 1992. **3**(1-2): p. 61-82.
55. Lynn, A.K. and W. Bonfield, *A Novel Method for the Simultaneous, Titrant-Free Control of pH and Calcium Phosphate Mass Yield.* Accounts of Chemical Research, 2005. **38**(3): p. 202-207.
56. Hafez, I.T., et al., *Calcium Phosphate Overgrowth on Silicate Sand.* Crystal Growth & Design, 2006. **6**(3): p. 675-683.
57. Funda, T., et al., *Predicting the chemical composition of juvenile and mature woods in Scots pine (Pinus sylvestris L.) using FTIR spectroscopy.* Wood Science and Technology, 2020. **54**(2): p. 289-311.
58. Garskaite, E., et al., *The Accessibility of the Cell Wall in Scots Pine (Pinus sylvestris L.) Sapwood to Colloidal Fe3O4 Nanoparticles.* ACS Omega, 2021.
59. Ronson, T.K. and A.J. McQuillan, *Infrared Spectroscopic Study of Calcium and Phosphate Ion Coadsorption and of Brushite Crystallization on TiO2.* Langmuir, 2002. **18**(12): p. 5019-5022.
60. Drouet, C., *Apatite formation: why it may not work as planned, and how to conclusively identify apatite compounds.* BioMed research international, 2013. **2013**: p. 490946.
61. Trpkovska, M., B. Šoptrajanov, and P. Malkov, *FTIR reinvestigation of the spectra of synthetic brushite and its partially deuterated analogues.* Journal of Molecular Structure, 1999. **480-481**: p. 661-666.
62. Mirković, M.M., et al., *Adsorption of malathion on mesoporous monetite obtained by mechanochemical treatment of brushite.* RSC Advances, 2016. **6**(15): p. 12219-12225.
63. Seki, T., et al., *The Bending Mode of Water: A Powerful Probe for Hydrogen Bond Structure of Aqueous Systems.* The Journal of Physical Chemistry Letters, 2020. **11**(19): p. 8459-8469.
64. Yu, C.-C., et al., *Vibrational couplings and energy transfer pathways of water's bending mode.* Nature Communications, 2020. **11**(1): p. 5977.
65. Pemberton, A.T., D.B. Magers, and D.A. King, *Integrated TGA, FTIR, and Computational Laboratory Experiment.* Journal of Chemical Education, 2019. **96**(1): p. 132-136.
66. Rotzinger, F.P., et al., *Structure and Vibrational Spectrum of Formate and Acetate Adsorbed from Aqueous Solution onto the TiO2 Rutile (110) Surface.* The Journal of Physical Chemistry B, 2004. **108**(16): p. 5004-5017.
67. Fengel, D., H. Jakob, and C. Strobel, *Influence of the Alkali Concentration on the Formation of Cellulose II. Study by X-Ray Diffraction and FTIR Spectroscopy.* 1995. **49**(6): p. 505-511.
68. Gebke, S., et al., *Flame Retardancy of Wood Fiber Materials Using Phosphorus-Modified Wheat Starch.* Molecules, 2020. **25**.
69. Dosen, A. and R.F. Giese, *Thermal decomposition of brushite, CaHPO4 center dot 2H(2)O to monetite CaHPO4 and the formation of an amorphous phase.* American Mineralogist, 2011. **96**(2-3): p. 368-373.
70. Frost, R.L. and S.J. Palmer, *Thermal stability of the 'cave' mineral brushite CaHPO4·2H2O – Mechanism of formation and decomposition.* Thermochimica Acta, 2011. **521**(1): p. 14-17.
71. Zhou, X., et al., *A Critical Review on Hemicellulose Pyrolysis.* Energy Technology, 2017. **5**(1): p. 52-79.
72. Yang, H., et al., *Characteristics of hemicellulose, cellulose and lignin pyrolysis.* Fuel, 2007. **86**(12): p. 1781-1788.

73. Viswanath, R.S. and P.J. Miller, *High temperature phase transition in NH4H2PO4.* Solid State Communications, 1979. **32**(8): p. 703-706.
74. Gao, N., et al., *TG–FTIR and Py–GC/MS analysis on pyrolysis and combustion of pine sawdust.* Journal of Analytical and Applied Pyrolysis, 2013. **100**: p. 26-32.
75. Bolarinwa, A., et al., *Cement casting of calcium pyrophosphate based bioceramics.* Advances in Applied Ceramics - ADV APPL CERAM, 2009. **108**.
76. Bigoni, D., et al., *Ceramics with the signature of wood: a mechanical insight.* Materials Today Bio, 2020. **5**: p. 100032.
77. Charrière, E., et al., *Mechanical characterization of brushite and hydroxyapatite cements.* Biomaterials, 2001. **22**(21): p. 2937-2945.
78. Konofalska, E., et al., *The Technical Quality of the Wood of Scots Pine (Pinus sylvestris L.) of Diverse Genetic Origin.* Forests, 2021. **12**(5).
79. Barthelat, F., Z. Yin, and M.J. Buehler, *Structure and mechanics of interfaces in biological materials.* Nature Reviews Materials, 2016. **1**(4): p. 16007.
80. Engstrand, J., C. Persson, and H. Engqvist, *The effect of composition on mechanical properties of brushite cements.* Journal of the Mechanical Behavior of Biomedical Materials, 2014. **29**: p. 81-90.
81. Hofmann, M.P., et al., *High-strength resorbable brushite bone cement with controlled drug-releasing capabilities.* Acta Biomaterialia, 2009. **5**(1): p. 43-49.
82. Moussa, H., et al., *High strength brushite bioceramics obtained by selective regulation of crystal growth with chiral biomolecules.* Acta Biomaterialia, 2020. **106**: p. 351-359.
83. 5660-1:2015, I., *Reaction to fire tests. Heat release, smoke production and mass loss rate. Part 1: Heat release rate (cone calorimeter method) and smoke production rate (dynamic measurement).* Reaction to fire tests. Heat release, smoke production and mass loss rate. Part 1: Heat release rate (cone calorimeter method) and smoke production rate (dynamic measurement), (2015).
84. Spearpoint, M.J. and J.G. Quintiere, *Predicting the piloted ignition of wood in the cone calorimeter using an integral model — effect of species, grain orientation and heat flux.* Fire Safety Journal, 2001. **36**(4): p. 391-415.
85. Marquis, D., E. Guillaume, and D. Lesenechal, *Accuracy (Trueness and Precision) of Cone Calorimeter Tests with and Without a Vitiated Air Enclosure.* Procedia Engineering, 2013. **62**: p. 103-119.
86. Kokkala, M.A., P.H. Thomas, and B. Karlsson, *Rate of heat release and ignitability indices for surface linings.* Fire and Materials, 1993. **17**(5): p. 209-216.
87. Wilkens Flecknoe-Brown, K. and P. van Hees, *Sensitivity analysis on the microscale combustion calorimeter for polyurethane foam using a full factorial design methodology.* Journal of Fire Sciences, 2018. **36**(6): p. 453-471.
88. Wilkens Flecknoe-Brown, K., *Fire behaviour of upholstered furniture component materials at multiple scales.* PhD Thesis, 2022. **Lund University**(2022).
89. Chai, G., et al., *On improving flame retardant and smoke suppression efficiency of epoxy resin doped with aluminum tri-hydroxide.* Advanced Composites Letters, 2019. **28**: p. 2633366X19894597.

Fig. 2. FE-SEM micrographs of the eggshell surface: (a) outer side consisting of the inorganic mineral, and (b) inner side showing membrane consisting of the organic matter.

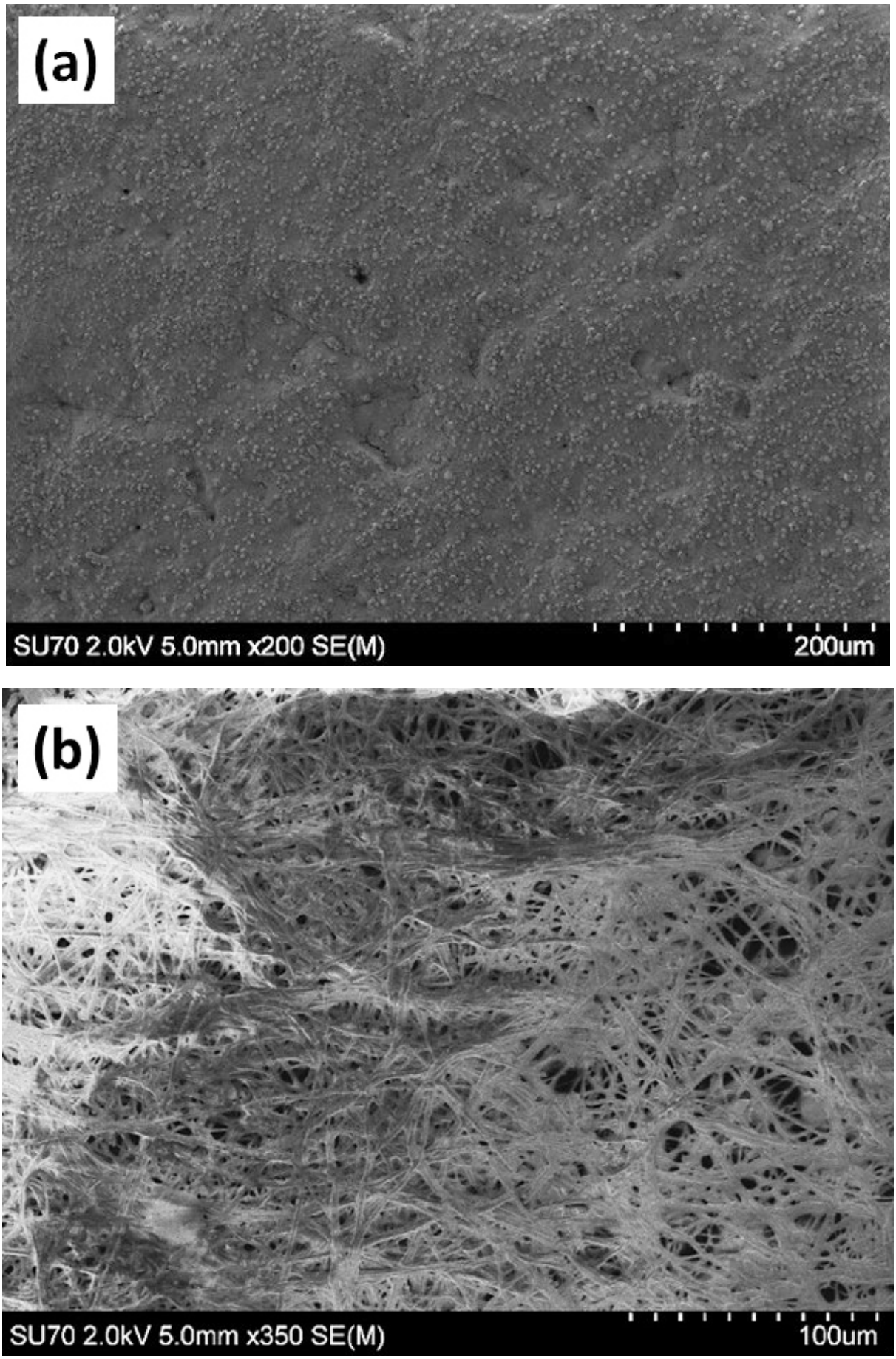

Fig. 7. (a-c) Cross-section SEM images showing morphological features of the mineral co-precipitated within Scots pine wood matrix as well as filling of the lumina, and (d) shows EDS spectrum of the mineral (studied place is shown in (c)).

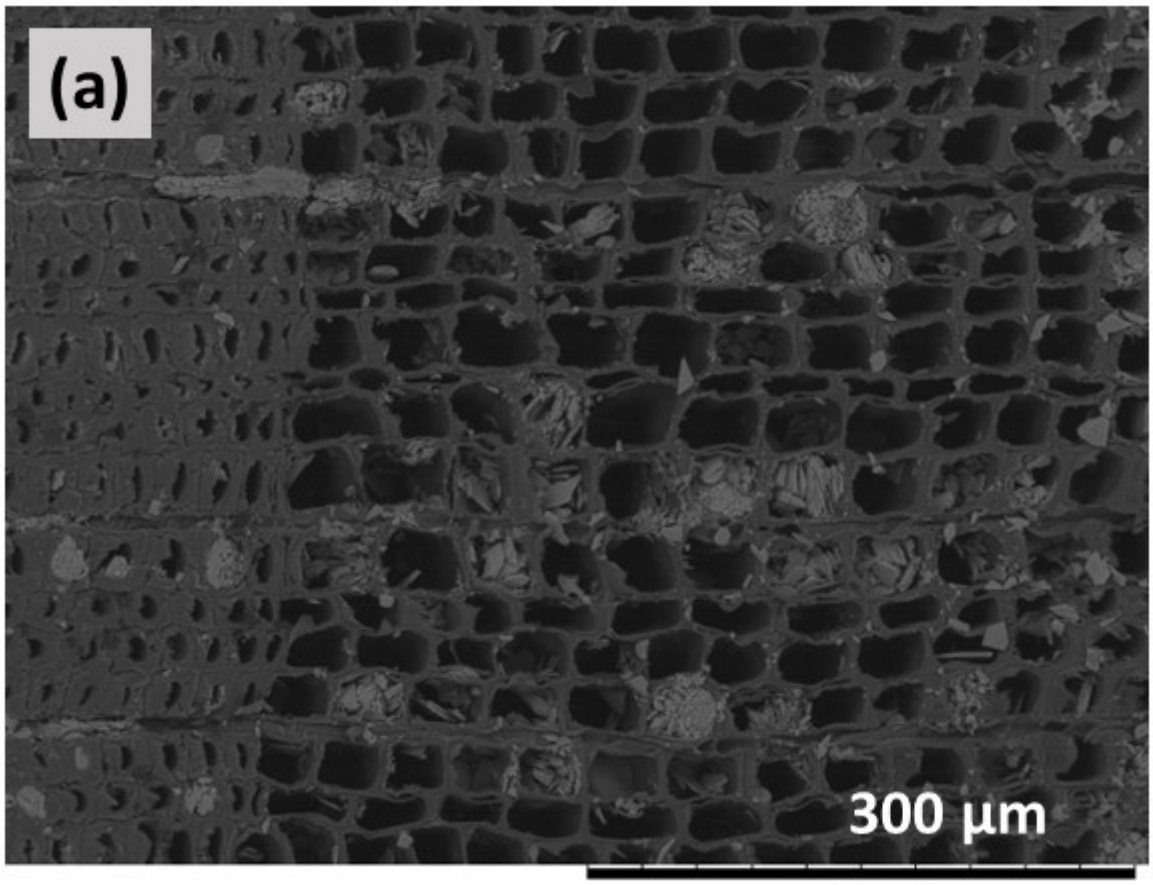

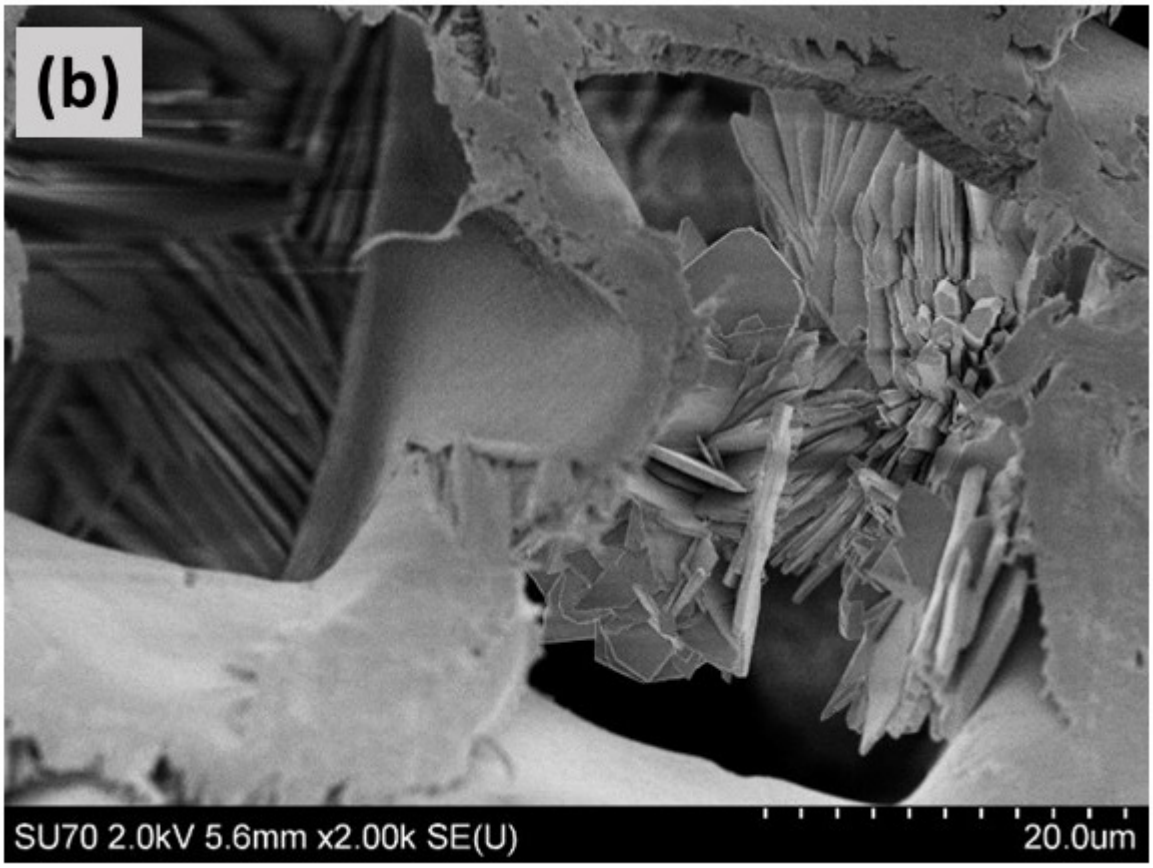

Page 12.

Fig. 7. (a-c) Cross-section SEM images showing morphological features of the mineral co-precipitated within Scots pine wood matrix as well as filling of the lumina, and (d) shows EDS spectrum of the mineral (studied place is shown in (c)).

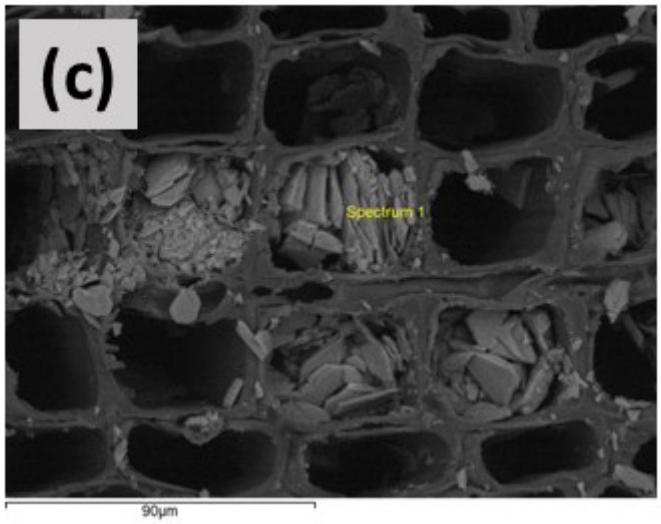

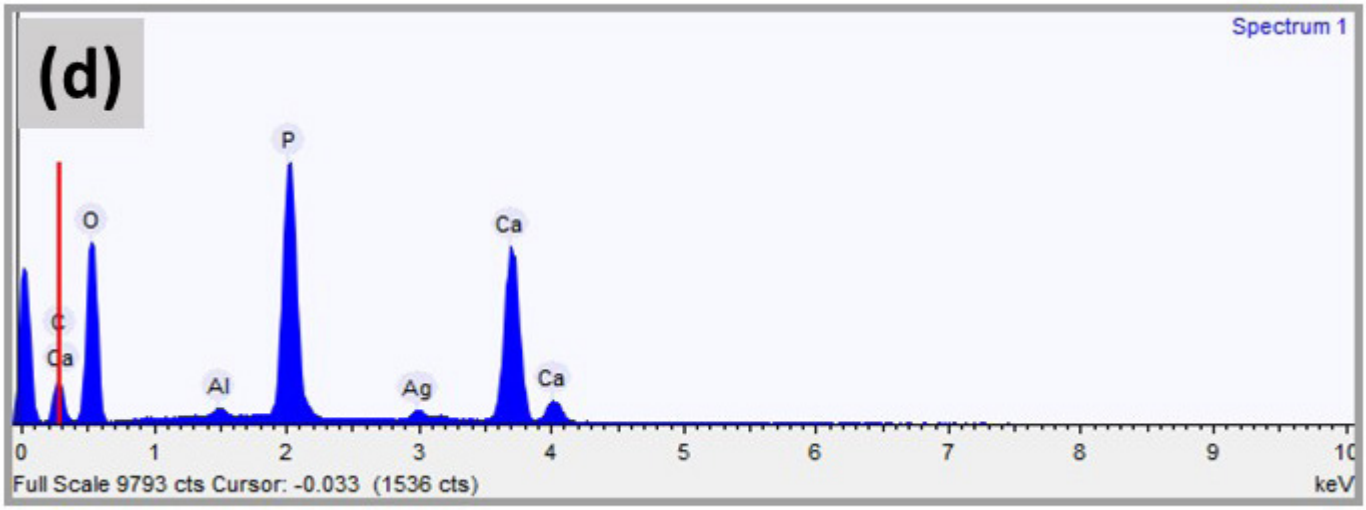

Page 13

Fig. 8. (a-h) SEM BEI (backscatter electron images) showing (a-g) EDS-based elemental mapping of wood mineralised from 0.5 M $Ca(CH_3COO)_2$/0.3 M $NH_4H_2PO_4$ solution system after the leaching tests and a distribution of individual elements (designated EDS mapping colours: Ca – red, P – green, O – blue; EDS-based elemental mapping images of Ca, P and C in grayscale are shown in (b), (d),and (f) images, respectively).

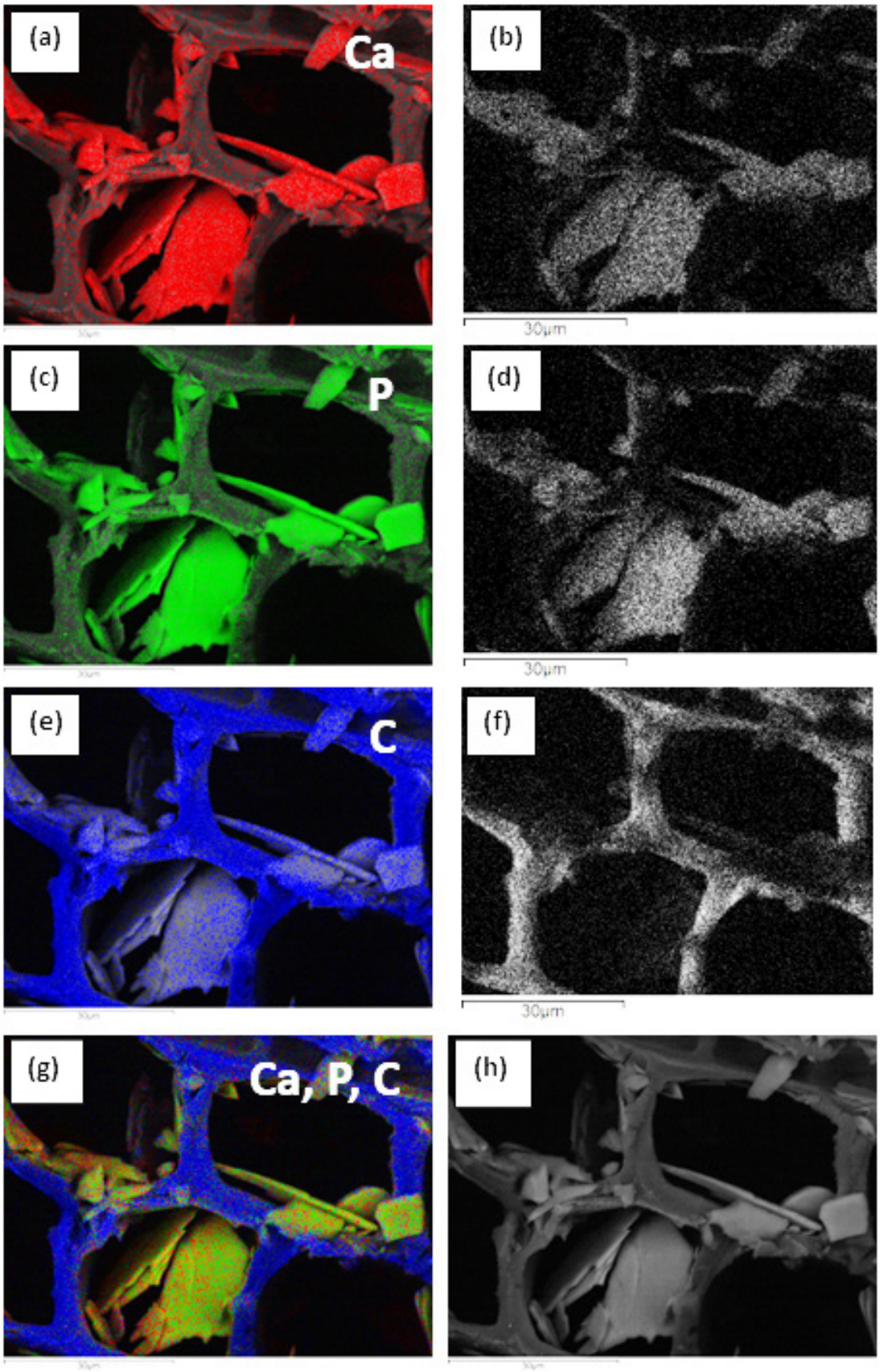

Fig. 11. FE-SEM micrographs of the wood mineralised from solutions of calcium acetate derived from eggshells and commercial $NH_4H_2PO_4$: (a) cross-sectional SEM micrograph of internal layer cut from 1x1x1 cm wood sample, and (b) shows surface of the wood block showing more mineral precipitated within wood matrix.

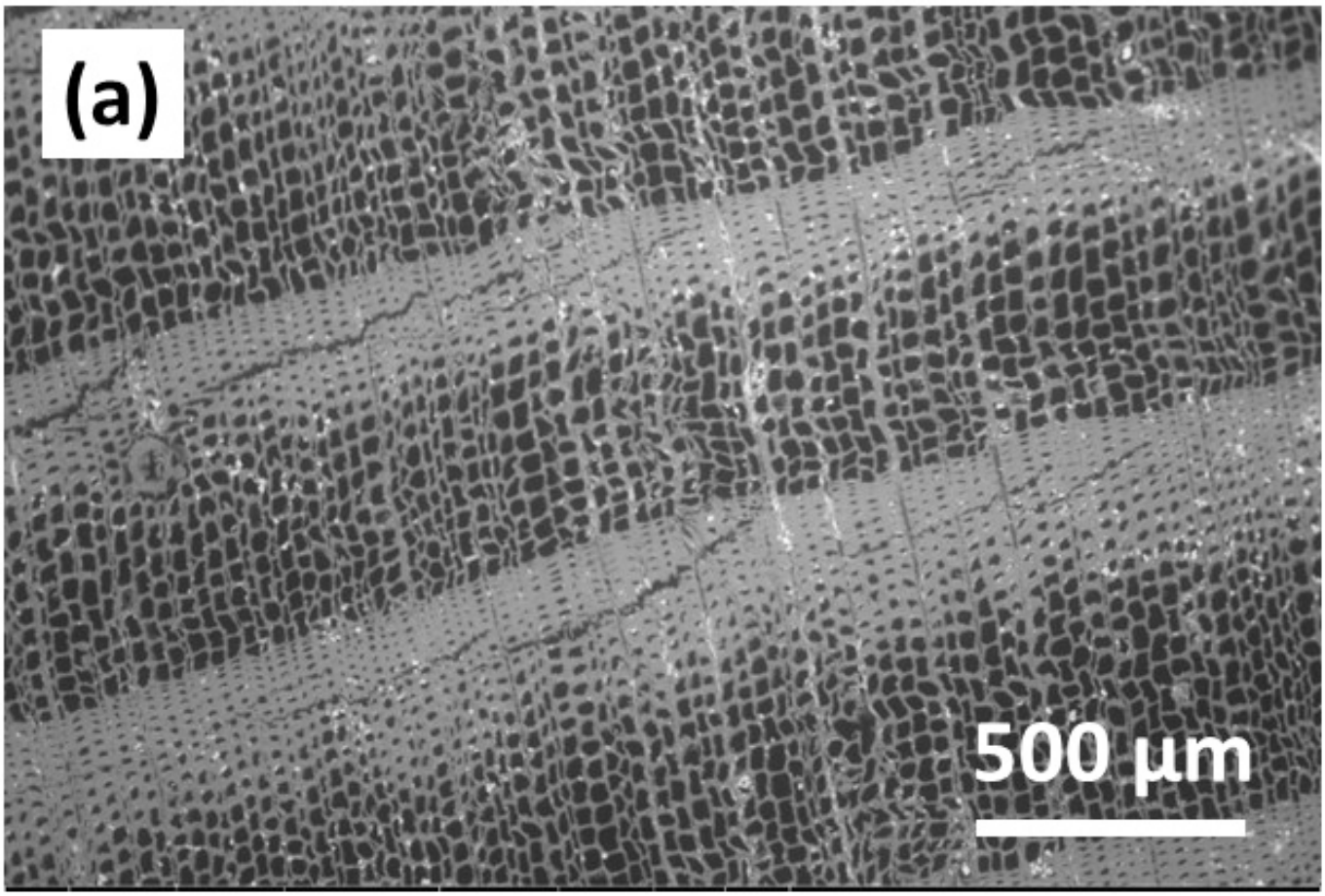

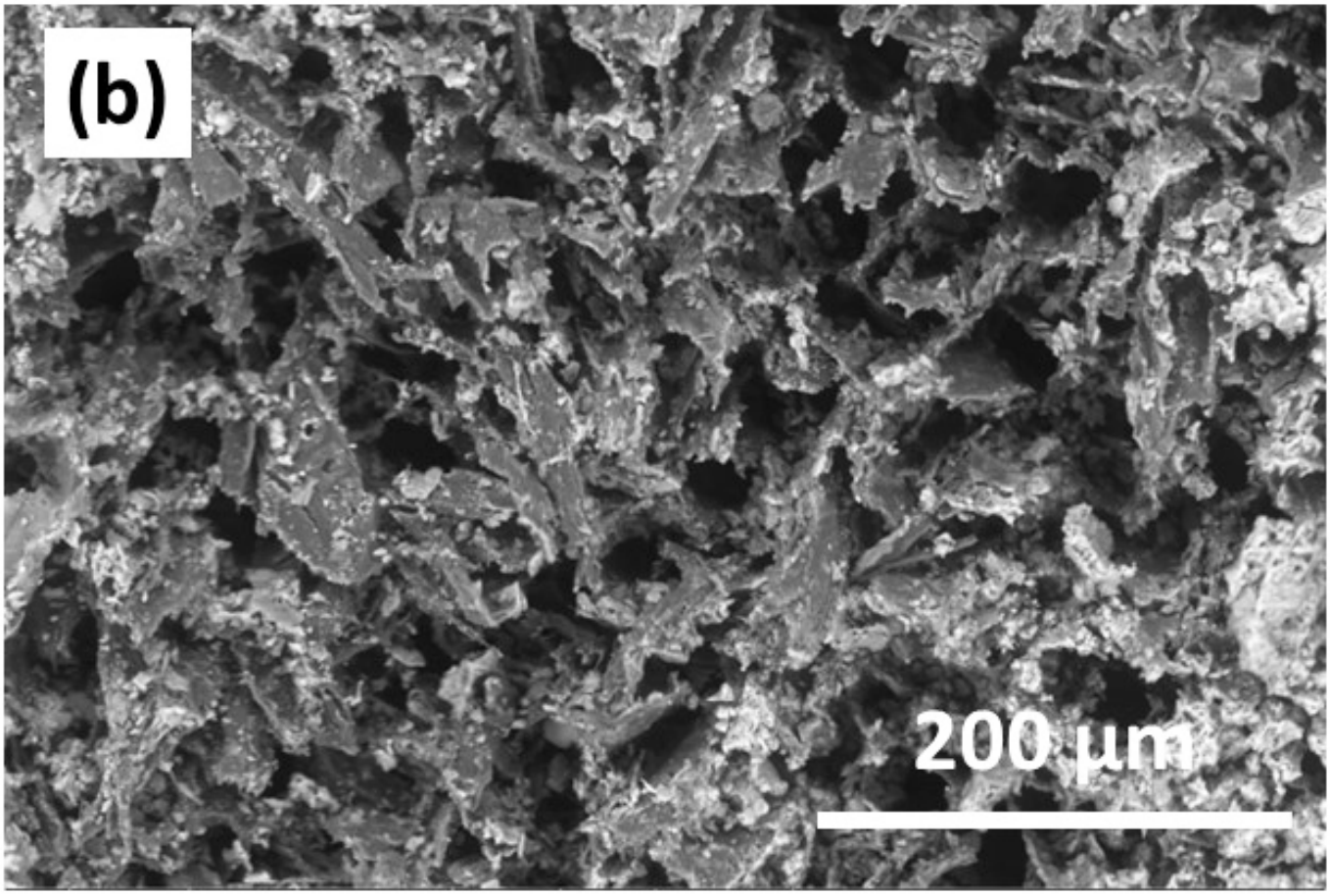

Page 18

Fig. 12. SEM/EDS mapping images of the HAP-mineralized Scots pine sapwood (microtome cut internal layer of the 1×1×1 cm cube were studied). Eggshell derived from 0.5 M concentration.

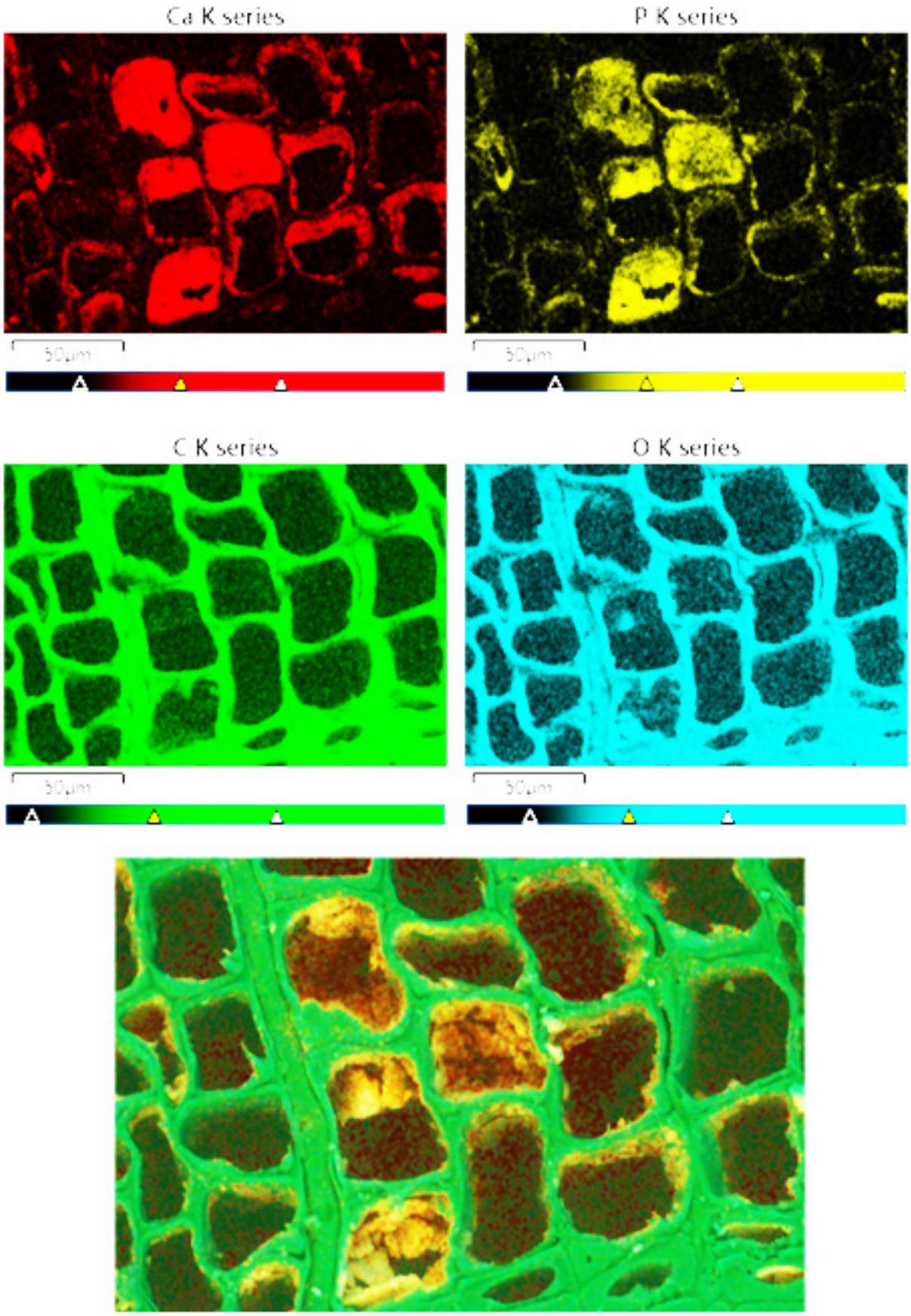

Support organisations

This project was funded 2021 by the organizations below

Akademiska hus • Bengt Dahlgren Brand & Risk • BIV Föreningen för Brandteknisk Ingenjörsvetenskap • Brand och Bygg Sverige AB • Brandkåren Attunda Brandskyddsföreningen Gävleborg • Brandskyddsföreningen Skaraborg Brandskyddsföreningen Södermanland • Brandskyddsföreningen Värmland Brandskyddsföreningen Väst • Brandskyddsföreningen Västernorrland Brandskyddslaget • Dina Gruppen • Eld & Vatten • Folksam • Fortifikationsverket Försäkrings AB Göta Lejon • GellCon • If Skadeförsäkring • Kammarkollegiet Kingspan Insulation AB • Kiruna Räddningstjänst • Kristianstads Räddningstjänst Kommunassurans Syd Försäkrings AB • Kyrkans försäkring • Lantmännen MSB, myndigheten för samhällsskydd och beredskap • NBSG, Nationella Brandsäkerhetsgruppen • Nerikes Brandkår • Region Stockholm Trafikförvaltningen Riksantikvarieämbetet • RISE, Research Instiutes of Sweden AB • Räddningstjänsten Boden • Räddningstjänsten Kalix • Räddningstjänsten Karlstadsregionen Räddningstjänsten i F-län/Räddsam F • Räddningstjänsten Luleå • Räddningstjänsten Oskarshamn • Räddningstjänsten Skinnskatteberg • Räddningstjänsten Skåne Nordväst Räddningstjänsten Syd • Räddningsstjänsten Östra Götaland • Räddningstjänsten Mitt Bohuslän • Scania CV AB • S:t Erik Försäkrings AB • Sirius International Stanley Security • Statens fastighetsverk • Sparia Försäkringsbolag Stockholms Stads Brandförsäkringskontor • Storstockholms Brandförsvar Sveriges brandkonsultförening • Swedisol • Södertörns brandförsvarsförbund Södra Dalarnas Räddningstjänstförbund • Södra Älvborgs räddningstjänstförbund Trafikverket • Trygg-Hansa • Uppsala brandförsvar • Värends Räddningstjänst Västra Sörmlands Räddningstjänst • Östra Skaraborg Räddningstjänst

The Swedish Fire Research Foundation - enables development of fire safety knowledge by research and other activities, and the spread of this knowledge to make a difference in our society.

This is possible trough raising money from all kinds of organisations with fire safety on their agenda as well as for altruistic reasons. The broad support from our society together with prosperous networks are key factors for our success.

Our mission is “A fire safe society built on knowledge”

Brandforsk
info@brandforsk.se, www.brandforsk.se

Project team

LULEÅ TEKNISKA UNIVERSITET

Financed by Brandforsk
Brandforsk's activities are made possible by support from various organizations in the community. Read more about our support organisations at www.brandforsk.se

BRAND FORSK